SUBMITTED TO J-PARC PAC

Towards a Long Baseline Neutrino and Nucleon Decay Experiment with a next-generation 100 kton Liquid Argon TPC detector at Okinoshima and an intensity upgraded J-PARC Neutrino beam

A.Badertscher[1], *A.Curioni*[1], *S.DiLuise*[1], *U.Degunda*[1], *L.Epprecht*[1], *L.Esposito*[1], *A.Gendotti*[1], *T.Hasegawa*[2], *S.Horikawa*[1], *L.Knecht*[1], *T.Kobayashi*[2], *C.Lazzaro*[1], *D.Lussi*[1], *A.Marchionni*[1], *A.Meregaglia*[1*], *T.Maruyama*[2], *G.Natterer*[1], *K.Nishikawa*[2], *F.Resnati*[1], *A.Rubbia*[1†], *C.Strabel*[1], *M.Tanaka*[2], *and T.Viant*[1]
(1) ETH Zurich, (2) KEK IPNS

December 18, 2009

Abstract
We envisage a new far detector composed of a 100 kton next-generation Liquid Argon Time Projection Chamber (LAr TPC) located underground in the region of Okinoshima (on D$\bar{o}$go, one of the Oki islands, in Shimane-ken, Japan). The Okinoshima location allows to detect the existing J-PARC neutrino beam at a baseline $L \sim 660$ km and an off-axis angle $\sim 0.76^o$ (longer baseline and more on-axis than the Kamioka region which has $L \sim 295$ km and an off-axis angle $\sim 2.5^o$). Assuming an upgrade of the J-PARC 30 GeV Main Ring operation from 750 kW to 1.66 MW, our goal is a high-statistics measurement of the $\nu_\mu \rightarrow \nu_e$ reaction (and possibly $\bar{\nu}_\mu \rightarrow \bar{\nu}_e$), with an emphasis on the 1st and 2nd flavor oscillation maxima, to determine the θ_{13} and δ_{CP} neutrino mixing matrix parameters. Five years neutrino operation would measure θ_{13} with $\delta(\sin^2 2\theta_{13}) \sim \pm 0.01$ and test CP-violation at better than 90% C.L. if θ_{13} had been previously detected in T2K, or otherwise improve the limit on θ_{13} by an order of magnitude ($\sin^2(2\theta_{13}) \lesssim 10^{-3}$ at 90%C.L.). For a value of δ_{CP} in the region of 90^o or 270^o, the statistical significance would exceed 3σ for $\sin^2(2\theta_{13}) \gtrsim 0.02$. These measurements rely on the opportunity offered by LAr TPC detectors to reconstruct neutrino events with high efficiency over a wide energy range, and with better energy-resolution and lower background compared to other large detector technologies. The detector will also simultaneously measure (anti)neutrinos from natural sources (atmospheric, supernova, etc.). In ten years of operation, proton and neutron lifetime sensitivities in the range $10^{34} - 10^{35}$ years will be reached, depending on the assumed final state channel. Our graded strategy towards the realization of the new far detector involves R&D activities at KEK and CERN and envisions future measurement campaigns on charged particle and neutrino beams at CERN and J-PARC, including the possible use of J-PARC K1.1BR beam and a new near location along the existing J-PARC neutrino beam.

1 Next generation accelerator based neutrino experiment beyond T2K

Large underground neutrino detectors, like SuperKamiokande [1,2], KAMLAND [3] and SNO [4], have achieved fundamental results in particle and astro-particle physics. A significant improvement in sensitivity for proton decays as well as the measurement of the unknown mixing angle θ_{13} and the prospects

*Now at IPHC, Université Louis Pasteur, CNRS/IN2P3, Strasbourg, France.
†Contact person: *andre.rubbia@cern.ch*.

to discover CP-violation in the leptonic sector, make clear that the next generation neutrino experiments will be more ambitious than previous ones. In this context, if a $\nu_\mu \rightarrow \nu_e$ conversion signal were to be observed at T2K [5], an immediate step forward to a next generation experiment aimed at the discovery of CP violation in the lepton sector would surely be recommended with high priority. Even in case that $\sin^2 2\theta_{13}$ is below the T2K sensitivity, the setup proposed here represents a time- and cost-effective way to continue exploring $\nu_\mu \rightarrow \nu_e$ conversion phenomenon with an order of magnitude better sensitivity than T2K. Similar arguments hold if hints for proton decay were found in the current round of experiments (see e.g. Ref. [6]).

Since several years, we contemplate a new giant next-generation and multi-purpose neutrino observatory based on the liquid Argon Time Projection Chamber (LAr TPC) technology of a total mass in the range of 100 kton [7–13], devoted to particle and astroparticle physics, providing new and unique scientific opportunities in this field, likely leading to fundamental discoveries.

The liquid Argon Time Projection Chamber (LAr TPC) is a powerful neutrino detector for uniform and high accuracy imaging of massive active volumes [14]. It is based on the fact that in highly pure Argon, ionization tracks can be drifted over distances of the order of meters. Imaging is provided by position-segmented electrodes at the end of the drift path, continuously recording the signals induced. Reference event timing (T_0) is provided by the prompt scintillation light.

Application of this technology, originally developed at CERN, to large detectors was pioneered by the ICARUS effort which culminated in the successful operation of the T600 on surface [15]. In its original design, the LAr TPC developed by ICARUS is however plagued by scalability problems. The main challenges for the extrapolation to the relevant mass scale are (a) very small signals (no amplification in liquid) (b) charge attenuation and diffusion along the drift path (c) large wire chambers in cryogenic environment.

Motivated by the necessity of massive detectors for neutrino physics and proton decay, several designs of large LAr detectors have therefore been discussed in the last several years (see Refs. [7, 13], [16], [17, 18], [19, 20]). The GLACIER design is a scalable concept for single volume very large detectors up to 100 kton: the cryostat is based on industrial liquefied natural gas (LNG) technology and ionization imaging readout relies on the novel LAr LEM-TPC operated in double phase with charge extraction and amplification in the vapor phase.

Since 2008, ETHZ and KEK groups are collaborating towards the realization of a very large 100 kton-scale detector. A coherent R&D programme (see e.g. Refs. [21, 22]) is being performed in synergy and at two complementary locations: (1) at CERN (e.g. ArDM [23] is a fully instrumented detector of the GLACIER-design at the ton-scale, currently being commissioned at CERN with specific developments in the area of charge readout [24–26], light readout [27], electronics, very high voltage, cryogenics, LAr purification and recently large area LEM/THGEM developed in Collaboration with the CERN RD51 [28]) and (2) at KEK (e.g. the 10L operation and the 250L chamber being assembled at KEK).

Coupled to the J-PARC neutrino beam augmented with the anticipated increased intensity, the LAr TPC detector at Okinoshima would measure with unprecedented sensitivity the last unknown mixing angle θ_{13} and unveil the existence of CP violation in the leptonic sector, which in turn could provide an explanation of the matter-antimatter asymmetry in the Universe.

Compared with T2K experimental conditions, the new setup has the following benefits:

– (1) an improved J-PARC neutrino beam intensity and (2) an optimization of the baseline and of neutrino beam profile (the off-axis angle with respect to the neutrino source made possible by the very unique and favorable geography!); apart from the intensity upgrade, which will mostly represent an accelerator issue, no major modification of the existing beamline infrastructure is neither considered nor necessary[1];

[1] An optimization of the horn focusing optics might be considered at a later stage.

– an improved main far neutrino detector, including (1) the detection technology; (2) its mass. For instance, the powerful imaging is expected to offer excellent conditions to reconstruct with high efficiency electron events in the GeV range and above, while considerably suppressing the neutral current background mostly consisting of misidentified π^0's.

Being located deep underground and being very massive, the detector also provides a significant improvement in the sensitivity to search for proton decays, pursuing the only possible path to directly test physics at the GUT scale, extending the proton lifetime sensitivities up to $10^{34}-10^{35}$ years, depending on the assumed decay mode, i.e. in a range compatible with several theoretical models [11]; moreover it will detect neutrinos as messengers from astrophysical objects as well as from the Early Universe to give us information on processes happening in the Universe, which cannot be studied otherwise. In particular, it will sense a large number of neutrinos emitted by exploding galactic and extragalactic type-II supernovae, allowing an accurate study of the mechanisms driving the explosion [8]. The neutrino observatory will also perform precision studies of other astrophysical or terrestrial sources of neutrinos like solar and atmospheric ones, and search for new sources of astrophysical neutrinos, like for example the diffuse neutrino background from relic supernovae or those produced in Dark Matter (WIMP) annihilation in the centre of the Sun or the Earth.

As a consequence, the same detector will provide us with an unique opportunity to address a long standing puzzle of our physical world, the “Quest for the Origin of Matter Dominated Universe" (see e.g. [29]), with the exploration of

– the Lepton Sector CP Violation by precise testing of the neutrino oscillation processes;
– Proton Decay.

The possibility to perform this experimental program in a European setting at one of the seven sites studied by the FP7 LAGUNA design study [30] and a new high-intensity neutrino beam from CERN, possibly involving synergies with the upgrade of the LHC injection chain, has also been investigated [31]. Here we focus on the opportunities offered at J-PARC.

2 J-PARC neutrino beam upgrade plan

As for the neutrino beam intensity improvement, the 30 GeV Main Ring (MR) power improvement scenario toward MW-class power frontier machine, KEK Roadmap plan, is analyzed and proposed by the J-PARC accelerator team as shown in Table 1.

Table 1: MR power improvement scenario toward MW-class power frontier machine (KEK Roadmap)

	Start Up	Next Step	**KEK Roadmap**
Power (MW)	0.1	0.45	**1.66**
Energy (GeV)	30	30	**30**
Rep. Cycle (sec.)	3.5	3-2	**1.92**
No. of Bunches	6	8	**8**
Particles/Bunch	1.2×10^{13}	$<4.1\times10^{13}$	$\mathbf{8.3\times10^{13}}$
Particles/Ring	7.2×10^{13}	$<3.3\times10^{14}$	$\mathbf{6.7\times10^{14}}$
LINAC (MeV)	181	181	**400**
RCS[a]	h=2	h=2 or 1	**h=1**

[a] Harmonic number of RCS

Accelerator component that must be modified or upgraded from their current status, toward the high intensity are listed in the following:

1. Number of bunches in MR should be increased from 6 to 8. For this purpose, fast rise time extraction kicker magnet have to be prepared. Its installation is foreseen in 2010 summer.
2. Repetition cycle of MR has to be improved from 3.5 seconds to 1.92 seconds. For this purpose RF and magnet power supply improvement is necessary.
3. RCS operation wih harmonic number 1 has to be conducted. This is to make the beam bunch to be longer in time domain to decrease space charge effect. For this purpose RF improvement is necessary. When RCS is operated with harmonic number 2, beam is injected to MR with 2 bunches $\times$ 4 cycles. On the other hand, when RCS is operated with harmonic number 1, beam is injected to MR with single bunch with doubled number of protons $\times$ 8 cycles.
4. LINAC 400 MeV operation is required to reduce space charge effects at RCS injection. Construction of necessary component is already approved and started.

The upgrade of the beam intensity can proceed in parallel with the construction and commissioning of the new far detector.

3 Far detector options: How to approach Lepton Sector CP Violation

The primary motivation of T2K [5] is to find an excess of electron-like events above backgrounds, compatible with $\nu_\mu \rightarrow \nu_e$ conversion phenomenon in the atmospheric regime, with a sensitivity by about an order of magnitude in the mixing angle $\sin^2 2\theta_{13}$ compared to the CHOOZ experimental limit [32]. The discovery of a non-vanishing θ_{13} angle would ascertain the 3×3 nature of the lepton flavor mixing matrix. In case of negative result, which might indicate that some symmetry is constraining θ_{13} to be close to zero, the determination of θ_{23} might shed some light by understanding how much the angle is close to being maximal.

The PAC approved program for T2K is to accumulate an integrated proton power on target of 0.75 MW$\times 5 \times 10^7$ seconds. Within a few years of run, critical information, which will guide the future direction of the neutrino physics, will be obtained based on the data corresponding to about 1 to 2 MW$\times 10^7$ seconds integrated proton power on target (roughly corresponding to a 3σ discovery at $\sin^2 2\theta_{13} >$ 0.05 and 0.03, respectively).

The neutrino flavor oscillation probability including atmospheric, solar and interference terms, as well as matter effects, can expressed using the following equation [33–35]

$$P(\nu_e \rightarrow \nu_\mu) \sim \sin^2 2\theta_{13} \cdot T_1 + \alpha \cdot \sin\theta_{13} \cdot (T_2 + T_3) + \alpha^2 \cdot T_4. \quad (1)$$

where,

$$\begin{aligned} T_1 &= \sin^2\theta_{23} \cdot \frac{\sin^2[(1-A)\cdot\Delta]}{(1-A)^2} \\ T_2 &= \sin\delta_{CP} \cdot \sin 2\theta_{12} \cdot \sin 2\theta_{23} \cdot \sin\Delta \frac{\sin(A\Delta)}{A} \cdot \frac{\sin[(1-A)\Delta]}{(1-A)} \\ T_3 &= \cos\delta_{CP} \cdot \sin 2\theta_{12} \cdot \sin 2\theta_{23} \cdot \cos\Delta \frac{\sin(A\Delta)}{A} \cdot \frac{\sin[(1-A)\Delta]}{(1-A)} \\ T_4 &= \cos^2\theta_{23} \cdot \sin^2 2\theta_{12} \frac{\sin^2(A\Delta)}{A^2}. \end{aligned} \quad (2)$$

where $\alpha \equiv \frac{\Delta m^2_{21}}{\Delta m^2_{31}}$, $\Delta \equiv \frac{\Delta m^2_{31} L}{4E}$, $A \equiv \frac{2\sqrt{2} G_F n_e E}{\Delta m^2_{31}}$. $\Delta m^2_{31} = m^2_3 - m^2_1$, $\Delta m^2_{21} = m^2_2 - m^2_1$, θ_{13} is the mixing angle of the 1st and 3rd generations, while θ_{12} is that for 1st and 2nd, and θ_{23} is that for 2nd and 3rd generations.

From the analysis of this expression, it can be noted that the effects of the CP phase δ_{CP} appear either [12]:

– a difference between ν and $\bar{\nu}$ behaviors (this method is sensitive to the CP-odd term which vanishes for $\delta = 0$ or 180°);
– or in the energy spectrum shape of the appearance oscillated ν_e charged current events (sensitive to all the non-vanishing δ values including 180°).

It should be noted that if one precisely measures the ν_e appearance energy spectrum shape (peak position and height for 1st and 2nd oscillation maximum and minimum) with high resolution, CP effect could be investigated with neutrino run only. Antineutrino beam conditions are known to be more difficult than those for neutrinos (lower beam flux due to leading charge effect in proton collisions on target, small antineutrinos cross-section at low energy, etc.).

Figure 1 (left) shows neutrino flux for vaious off-axis angles. If one selects an almost on-axis

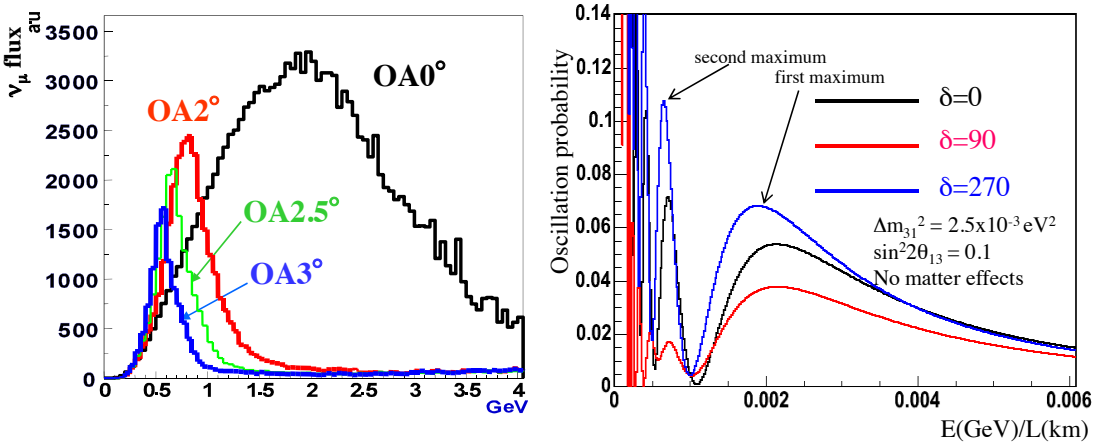

Fig. 1: Neutrino flux for various off-axis angle (left) and Probability for $\nu_\mu \rightarrow \nu_e$ oscillations as a function of the E(GeV)/L(km) for various δ. (right)

setting, a rather wide energy coverage is obtained, which allows to cover the 1st and 2nd maximum simultaneously. In order to work in the wide-band condition, the π^0 background originating from high energy neutrinos must be treated with high discrimination ability against genuine electrons. This is why we focus on the large LAr TPC. A lack of discrimination against the π^0 background is hardly exchangeable with a higher statistics.

Figure 1 (right) shows the oscillation probability as a function of the E(GeV)/ L(km). If the distance between source and detector is fixed, the curves can be easily translated to that for the expected neutrino energy spectrum of the oscillated events. If the neutrino energy spectrum of the oscillated events can be reconstructed with sufficiently good resolution in order to distinguish first and second maximum, useful information to extract the CP phase is available, even only with a neutrino run. The baseline must be long enough to measure the 2nd oscillation maximum. In longer baselines, the statistical significance for a given beam profile will get worse and the measurement will be affected by matter effects, but for baselines less than 1000 km these latter remain small.

4 J-PARC to Okinoshima Long Baseline Neutrino Experiment

Our proposal is "J-PARC to Okinoshima Long Baseline Neutrino Experiment" [12]. The layout of the envisioned experiment is shown in Figure 2. With the same configuration as T2K (2.5° off-axis angle), the center of the neutrino beam will go through underground beneath SK (295 km baseline), and will automatically reach the Okinoshima island region (658 km baseline) with an off-axis angle 0.76° (almost on-axis).

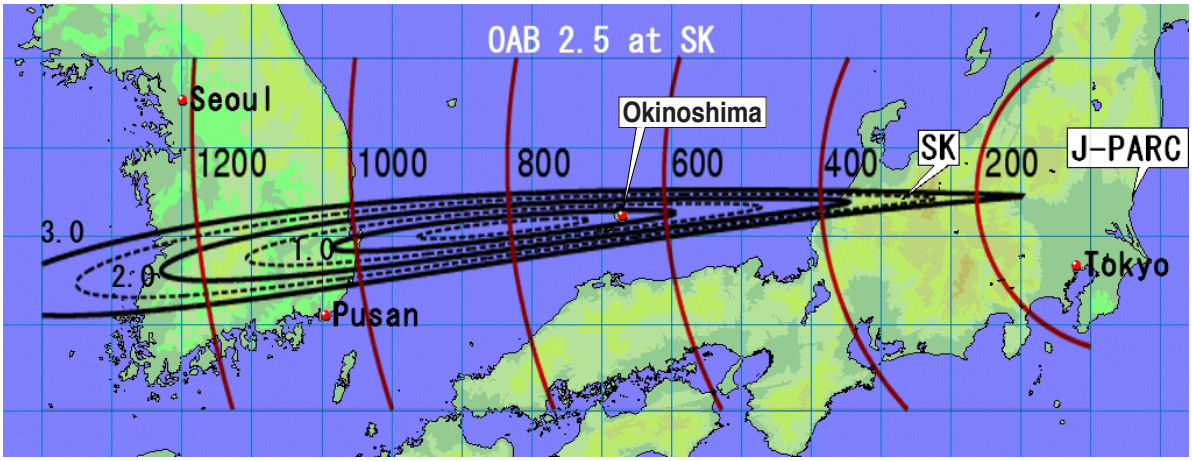

Fig. 2: J-PARC to Okinoshima Long Baseline Neutrino Experiment (figure adapted from `http://www2.yukawa.kyoto-u.ac.jp/~okamura/`).

In order to cover a wider energy range, detector location which is near on-axis is favored. If one assumes that the second oscillation maximum has to be located at an energy larger than about 400 MeV, the baseline should be longer than about 600 km. In addition, in order to collect enough statistics given the beam, baseline should not be too much longer than above stated. Taking into account all of the above mentioned considerations, the Okinoshima region turns out to be ideal.

4.1 Neutrino flux, expected event rates and energy spectrum of ν_e charged current events

Detector is taken to have a mass of 100 kton and the π^0 background is expected to be highly suppressed thanks to the fine sampling granularity of the readout, hence the dominant irreducible background is the intrinsic ν_e component of the beam.

Analysis is based on the assumption of using a neutrino run only during five years (reasonable time duration with 10^7 seconds running period/year), under the best J-PARC MR beam assumption. An anti-neutrino beam (opposite horn polarity) might be considered in a second stage in order to cross-check the results obtained with the neutrino run (in particular for CP and mass hierarchy parameter correlations).

According to the KEK Roadmap, the performance of the MR accelerator and the integrated exposure are taken as follows:

- The average beam power is reaching 1.66 MW;
- The kinetic energy of the incident protons is 30 GeV;
- A total of 3.45×10^{21} POT is delivered on target per year;
- A run lasting five years operation with horn setting to neutrino mode.

The parameters of the Okinoshima location are as follows:

- Distance from J-PARC is 658 km;
- The axis of the beam is off by 0.76°;

The expected neutrino flux calculated under these assumptions is shown in Figure 3 where the curves correspond to one year run (3.45×10^{21} POT). The black, red, green, blue lines show ν_μ, $\bar{\nu}_\mu$, ν_e, $\bar{\nu}_e$ fluxes, respectively. The interacting neutrino cross section on Argon was computed using the NUANCE programme [36]. We use the followings parameters for the cross section calculation:

– Number of protons is 18, and that of neutrons is 22.
– Medium density is 1.4 g/cm^3.
– Nucleus Fermi Gas model with binding energy of 30 MeV and Fermi momentum of 242 MeV/c.

Taking these into account, we obtain the neutrino cross section shown in Figure 4.

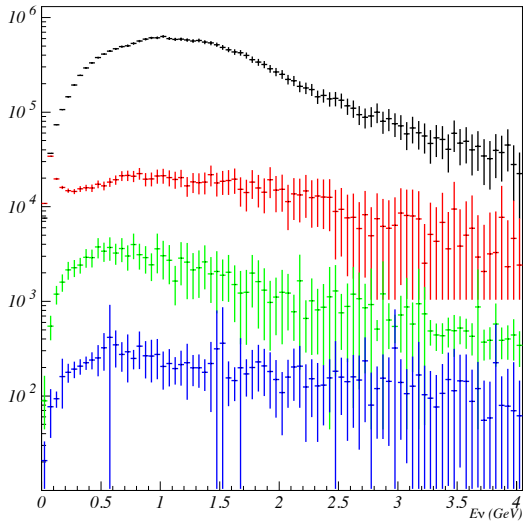

Fig. 3: Calculated neutrino flux under the assumptions (3.45×10^{21} POT). Black shows ν_μ, red shows $\bar{\nu}_\mu$, green shows ν_e, blue shows $\bar{\nu}_e$ fluxes, respectively.

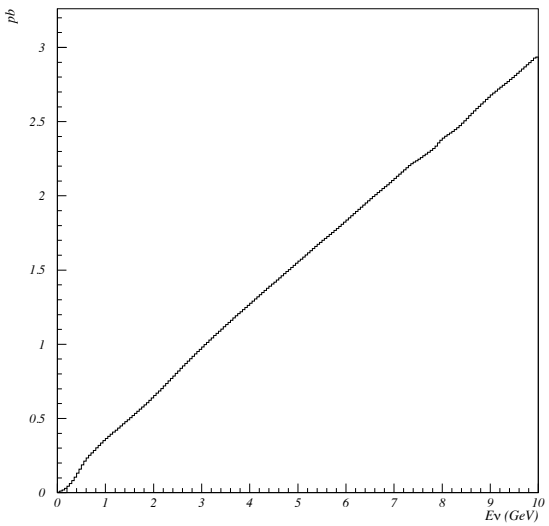

Fig. 4: Calculated neutrino-Argon cross section, unit by pb. Nuclear effects are taken into account.

Table 2 shows that total number of charged current (CC) events at Okinoshima for the null oscillation case and the number of CC ν_e events from $\nu_\mu \rightarrow \nu_e$ oscillations for three different mixing angles, and in various δ_{CP} scenarios, normalized to five years neutrino run at 1.66 MW and 100 kton fiducial mass. For definite calculations, we use the following parameters (we assume that most of these parameters will be precisely measured within the timescale of the one discussed here):

– θ_{23} is $\pi/4$.
– θ_{12} is 0.572904 rad.
– Δm^2_{21} is 8.2×10^{-5} eV^2.

Events for 100 kton at Okinoshima normalized to 5 years at 1.66 MW beam power				
	ν_μ	ν_e	$\bar{\nu}_\mu$	$\bar{\nu}_e$
Beam components (null oscillation)	82000	750	1460	35
$\nu_\mu \rightarrow \nu_e$ oscillations				
δ_{CP} =	0°	90°	180°	270°
$\sin^2 2\theta_{13} = 0.1$	2867	2062	2659	3464
$\sin^2 2\theta_{13} = 0.05$	1489	1119	1342	1908
$\sin^2 2\theta_{13} = 0.03$	942	506	829	1266

Table 2: Number of CC events at Okinoshima: beam components for null oscillation, and oscillated events in various δ_{CP} scenarios (normalized to five years neutrino run)

– $|\Delta m^2_{31}|$ is 2.5×10^{-3} eV^2.
– Earth density for matter effects are 2.8 g/cm^3.
– normal hierarchy is assumed unless mentioned otherwise.

Figure 5 shows the energy spectra of electron neutrino (with perfect resolution) at the cases of δ_{CP} equal 0°, 90°, 180°, 270°, respectively. Shaded region is common for all plots and it shows the background from beam ν_e. As shown, the value of δ varies the energy spectrum, especially the first and the second oscillation peaks (heights and positions), therefore comparison of the peaks determine the value δ, while the value of $\sin^2 2\theta_{13}$ changes number of events predominantly.

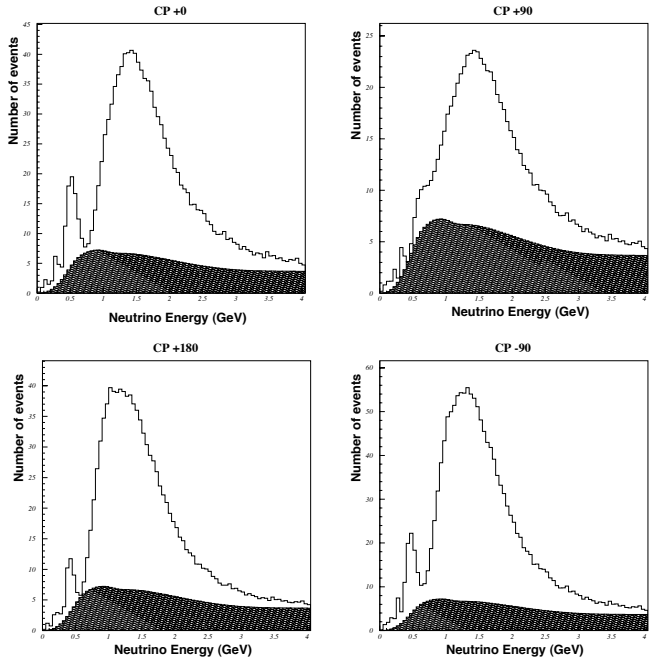

Fig. 5: Energy spectra at $\sin^2 2\theta_{13}$=0.03 case, but δ_{CP} = 0° (top-left), 90° (right-top), 180° (left-bottom), 270° (right-bottom) cases.

4.2 Oscillation parameters measurement from energy spectrum analyses

Assuming all others were measured very precisely, there are only two free parameters $\sin^2 2\theta_{13}$ and δ_{CP} to be fitted using the energy spectra. As shown in Figure 1(rignt), the value of δ_{CP} varies the energy spectrum, especially the first and the second oscillation peaks (heights and positions), therefore comparison of the peaks determine the value δ_{CP}, while the value of $\sin^2 2\theta_{13}$ changes number of events predominantly.

To fit the free parameters, a binned likelihood method is used. The Poisson bin-by-bin probability of the observed data from the expected events (for an assumed pair of values ($\sin^2 2\theta_{13}$, δ_{CP})) is calculated. The fit procedure is validated by testing the result on a pseudo-experiment.

At this stage, we only take statistical uncertainty into account for the fitting, thus other systematic uncertainties like far/near ratio, beam ν_e shape, energy scale, and so forth are not considered. Also, oscillated signal and beam ν_e are only accounted in the fit, i.e. other background like neutral current π^0 or beam $\bar{\nu}_e$ contamination is assumed to be negligible compared to beam ν_e contamination.

As a reference, we extract allowed regions in the perfect resolution case (See Figure 6). Twelve allowed regions are overlaid for twelve true values, $\sin^2 2\theta_{13}$=0.1, 0.05, 0.02, and δ_{CP}=0°, 90°, 180°,

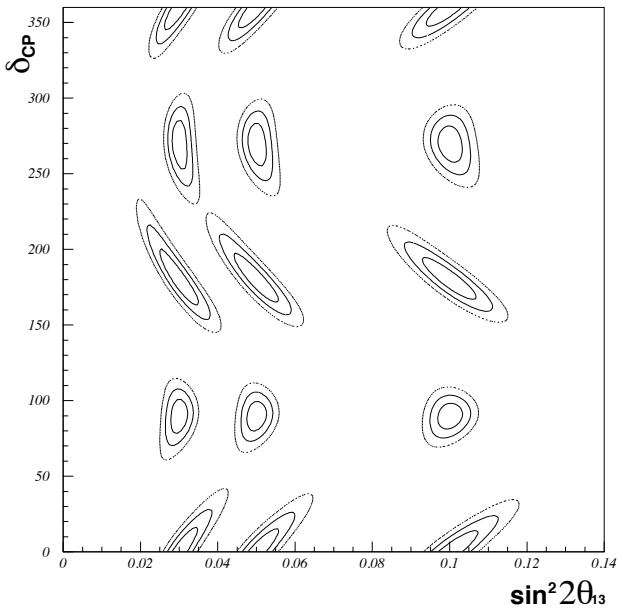

Fig. 6: Allowed regions in the perfect resolution case. Twelve allowed regions are overlaid for twelve true values, $\sin^2 2\theta_{13}$=0.1, 0.05, 0.02, and δ_{CP}=0°, 90°, 180°, 270°, respectively.

270°, respectively. The δ_{CP} sensitivity is 20∼30° depending on the true δ_{CP} value.

4.3 Mass hierarchy degeneracy

The influence of matter on neutrino oscillations was first considered by Wolfenstein [37]. As is well-known (although never directly experimentally verified), oscillation probabilities get modified under these conditions. Matter effects are sensitive to the neutrino mass ordering and different for neutrinos and antineutrinos. As mentioned earlier, we consider in this paper the possibility of a neutrino-only run. Hence, we briefly address in this section the question of normal hierarchy (NH) versus inverted hierarchy (IH). Since we are focusing on the potential discovery of CP-violation in the leptonic sector, our discussion is geared towards possible ambiguities that would arise if the mass hierarchy was unknown.

Indeed, Figure 7 illustrates the results of a fit of a pseudo-data with NH by both NH (black) and IH (red) hypotheses, assuming only the neutrino run. The best fit likelihood value with one assumed hierarchy is used to calculate the likelihood variation ΔL for both hierarchies. One could claim that CP-violation is discovered if the experimental results of a given experiment exclude the δ_{CP} phase to be either 0 or 180°. Hence, the danger is that the lack of knowledge of the mass hierarchy (or rather the "wrong" choice in hypothesis when selecting the hierarchy in the fit of the data), gives a result for δ_{CP} consistent with either 0 or 180°. On the other hand, if fits of a given experiment with both assumed hierarchies provide neither 0 nor 180°, one can declare "discovery" although the mass hierarchy could not be determined. Alternatively, if it turned out in the actual experiment that one of results of the fit is consistent with $\delta_{CP} = 0$ or 180°, one would still have the possibility to consider an anti-neutrino run in order to solve this ambiguity.

Our results indicate that CP-violation would be unambiguously discovered under our assumption for true values of δ_{CP}'s in the region of 90° and 270°. Alternatively, in case of true values of δ_{CP}'s near 0° or 180° an antineutrino flux would help untangle the two solutions if the neutrino mass hierarchy was unknown.

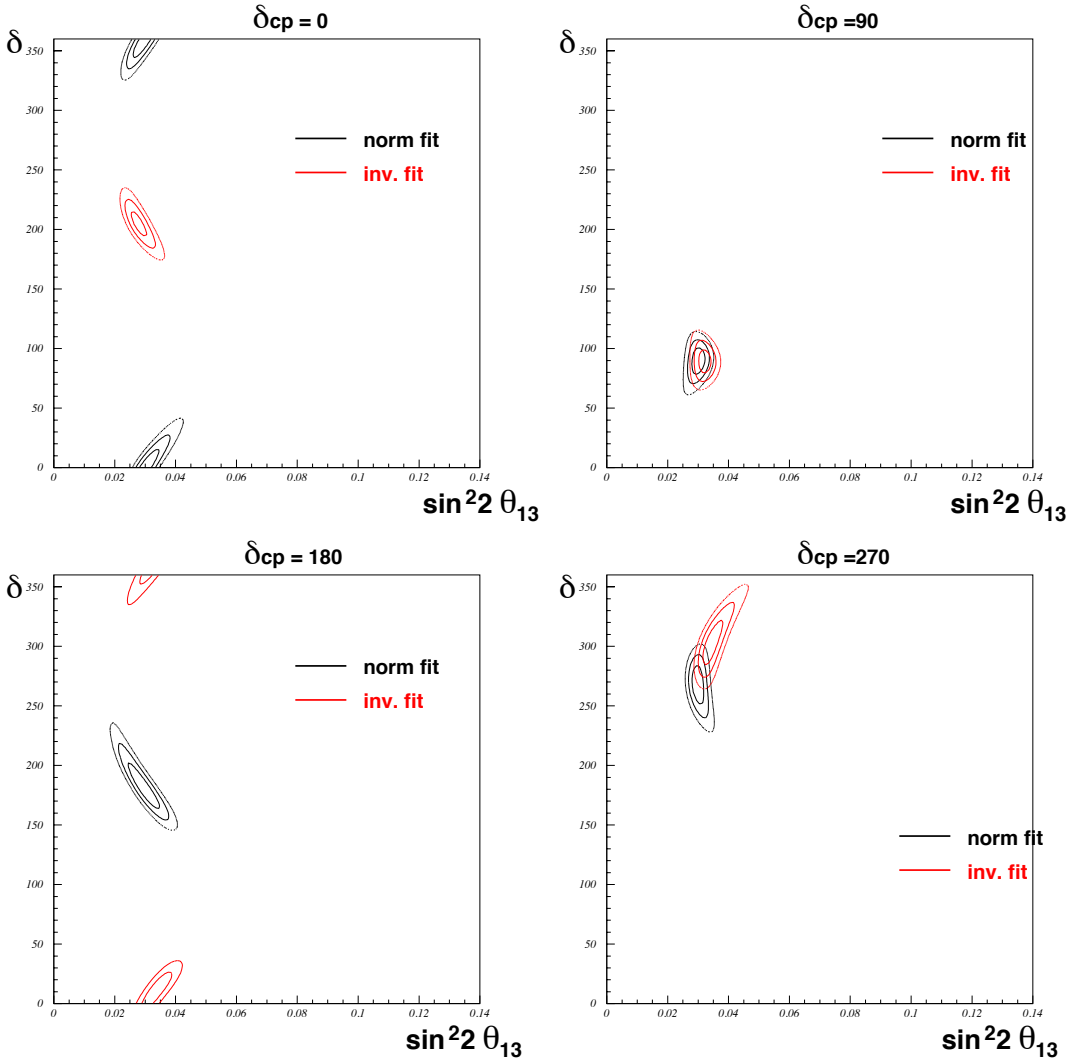

Fig. 7: Mass hierarchy investigation with neutrino run only. If fits with both hierarchy hypotheses provide neither 0 nor 180°, one can declare discovery of CP violation in the leptonic sector. If any of the fits results in a δ_{CP} of 0 or 180°, then an anti-neutrino run could be envisaged.

4.4 Expected sensitivity to $\sin^2 2\theta_{13}$

Although present study has focused on the possibility to measure the $\sin^2 2\theta_{13}$ and δ_{CP} oscillation parameters, it is instructive to estimate the sensitivity of the potential setup in the case of negative result from T2K. The corresponding sensitivity to discover θ_{13} in the true $(\sin^2 2\theta_{13}, \delta_{CP})$ plane at 90% C.L. and 3σ is shown in Figure 8.

In order to discover a non-vanishing $\sin^2 2\theta_{13}$, the hypothesis $\sin^2 2\theta_{13} \equiv 0$ must be excluded at the given C.L. As input, a true non-vanishing value of $\sin^2 2\theta_{13}$ is chosen in the simulation and a fit with $\sin^2 2\theta_{13} = 0$ is performed, yielding the "discovery" potential. This procedure is repeated for every point in the $(\sin^2 2\theta_{13}, \delta_{CP})$ plane.

At the 3σ C.L. the sensitivity of the T2K experiment is 0.02 [5]. Continuing to collect data at SK with an improved J-PARC neutrino beam for another 5 years would improve the T2K sensitivity by a factor ~ 2. In comparison, our simulations indicate that a 20 kton LAr TPC is expected to perform better than this although the masses are comparable, since the signal efficiency is higher than SK and the NC

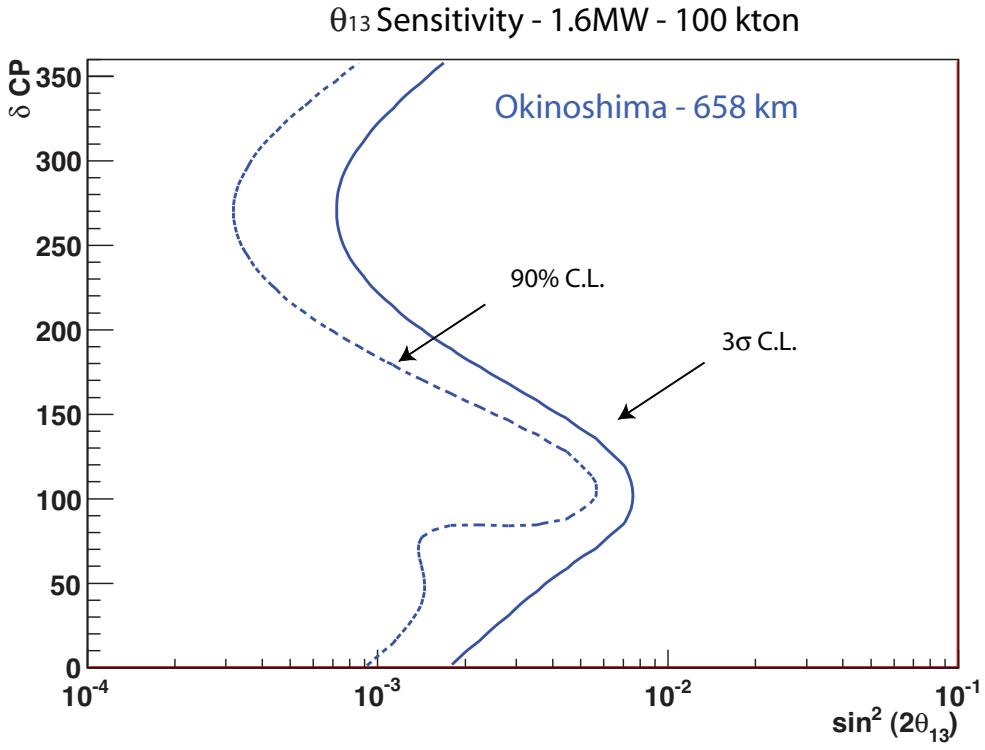

Fig. 8: Expected sensitivity to $\sin^2(2\theta_{13})$ for 5 years of neutrino run with 100 kton LAr at Okinoshima at 90%C.L. and 3σ.

background is assumed to be negligible contrary to SK. Even better, a 100 kton LAr TPC at Okinoshima would further improve the sensitivity by about a factor six compared to SK at Kamioka (or a factor 10 compared to T2K), thanks to its bigger mass, increased cross-section at higher energies and reduced off-axis angle, although the neutrino fluxes at the same off-axis angle would be reduced by a factor $\simeq 5$ because of the longer baseline.

5 Statistical significance of CP-discovery and mass hierarchy determination

While we stressed in the previous section the possibility to measure precisely the θ_{13} angle and δ_{CP} phase (positive measurement), we present in this section the customary sensitivity or discovery plots for CP and the mass hierarchy in the $(\sin^2 2\theta_{13}, \delta_{CP})$-plane. The expected sensitivities were computed with the help of the GLOBES [38] software, in a similar way to what we did previously which assumed a 100 kton liquid Argon detector (see Ref. [10] for details):

- In order to discover a non-vanishing $\sin^2 2\theta_{13}$, the hypothesis $\sin^2 2\theta_{13} \equiv 0$ must be excluded at the given C.L. As input, a true non-vanishing value of $\sin^2 2\theta_{13}$ is chosen in the simulation and a fit with $\sin^2 2\theta_{13} = 0$ is performed, yielding the "discovery" potential. This procedure is repeated for every point in the $(\sin^2 2\theta_{13}, \delta_{CP})$ plane. The corresponding sensitivity to discover θ_{13} in the true $(\sin^2 2\theta_{13}, \delta_{CP})$ plane at 90% C.L. and 3σ is shown in Figure 8.
- By definition, the CP-violation in the lepton sector can be said to be discovered if the CP-conserving values, $\delta_{CP} = 0$ and $\delta_{CP} = \pi$, can be excluded at a given C.L. The reach for discovering CP-violation is computed choosing a "true" value for δ_{CP} $(\neq 0)$ as input at different true values of $\sin^2 2\theta_{13}$ in the $(\sin^2 2\theta_{13}, \delta_{CP})$-plane, and for each point of the plane calculating the corresponding event rates expected in the experiment. This data is then fitted with the two CP-conserving

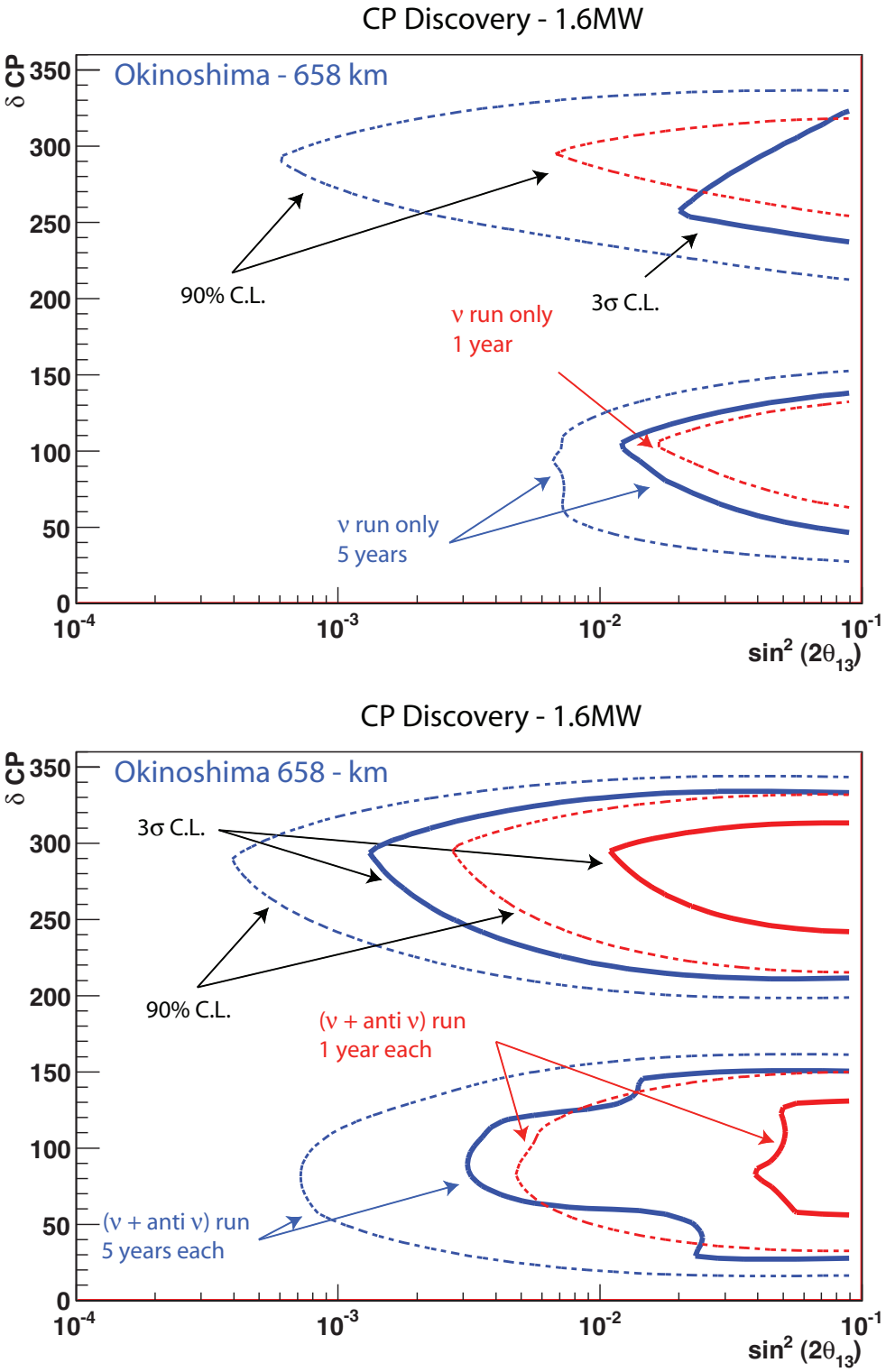

Fig. 9: Discovery potential for CP-violation at 90%C.L. and 3σ for (top) 1 resp. 5 years neutrino only (bottom) 1+1 resp. 5+5 years neutrino-antineutrino runs.

values $\delta_{CP} = 0$ and $\delta_{CP} = \pi$, leaving all other parameters free (including $\sin^2 2\theta_{13}$!). The opposite mass hierarchy is also fitted and the minimum of all cases is taken as final χ^2. The corresponding sensitivity to discover CP-violation in the true $(\sin^2 2\theta_{13}, \delta_{CP})$ plane is shown in Figure 9. The top plot shows the sensitivity with 1.6 MW beam power for 1 and 5 years of neutrino run; the bottom plot assumes 1 and 5 years of each neutrino and antineutrino runs.

– In order to determine the mass hierarchy to a given C.L., the opposite mass hierarchy must be excluded. A point in parameter space with normal hierarchy is therefore chosen as true value and the solution with the smallest χ^2 value with inverted hierarchy has to be determined by global minimization of the χ^2 function leaving all oscillation parameters free within their priors. The sensitivity to exclude inverted mass hierarchy in the true $(\sin^2 2\theta_{13}, \delta_{CP})$ plane is shown in Figure 10.

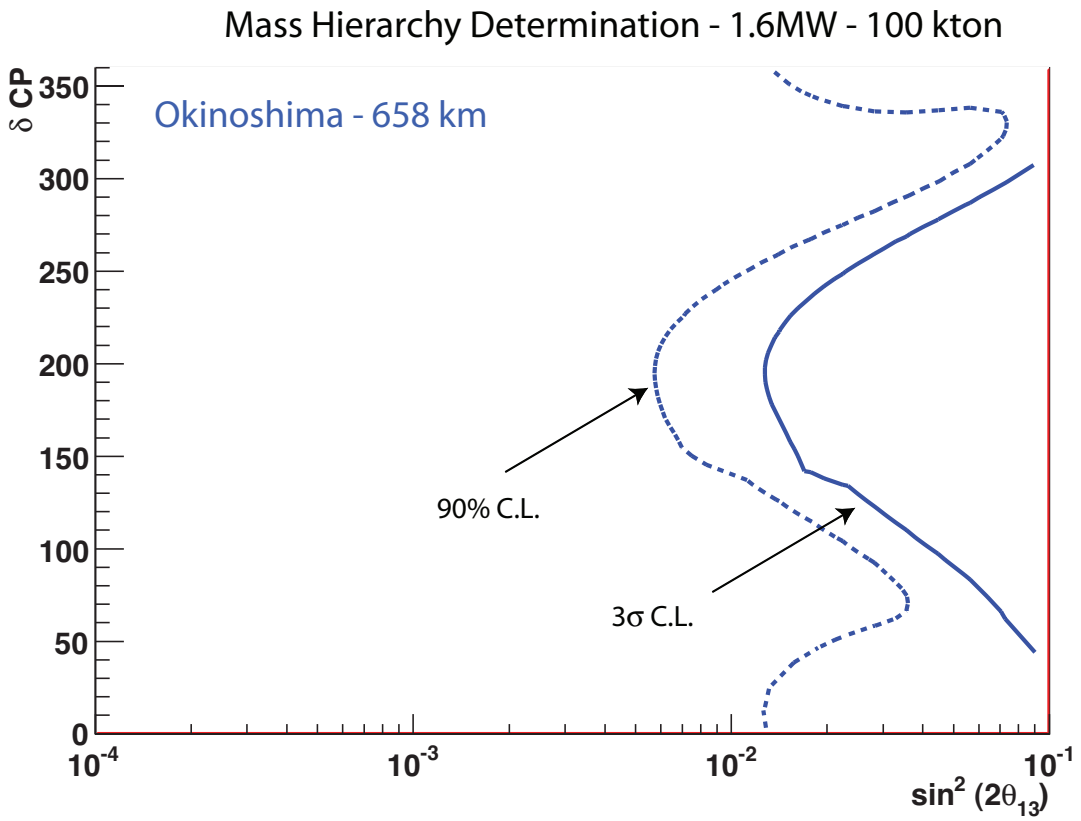

Fig. 10: Mass hierarchy discrimination at 90%C.L. and 3σ for 5+5 years neutrino-antineutrino runs.

Five years neutrino operation would measure θ_{13} with $\delta(\sin^2 2\theta_{13}) \sim \pm 0.01$ and test CP-violation at better than 90% C.L. if θ_{13} had been previously detected in T2K, or otherwise improve the limit on θ_{13} by an order of magnitude ($\sin^2(2\theta_{13}) \lesssim 10^{-3}$ at 90%C.L.). For a value of δ_{CP} in the region of 90^o or 270^o, the statistical significance would exceed 3σ for $\sin^2(2\theta_{13}) \gtrsim 0.02$. If θ_{13} were found in the neutrino run, adding 5 years of antineutrino run would allow to discover CP-violation at $> 3\sigma$ if $\sin^2(2\theta_{13}) > 10^{-2}$.

6 Proton decay discovery potential

Grand Unification of the strong, weak and electromagnetic interactions into a single unified gauge group is an extremely appealing idea [39, 40] which has been vigorously pursued theoretically and experimentally for many years. The detection of proton or bound-neutron decays would represent its most

direct experimental evidence. The physics potentialities of very large underground Liquid Argon TPC was recently carried out with detailed simulation of signal efficiency and background sources, including atmospheric neutrinos and cosmogenic backgrounds [11]. It was found that a liquid Argon TPC, offering good granularity and energy resolution, low particle detection threshold, and excellent background discrimination, should yield very good signal over background ratios in many possible decay modes, allowing to reach partial lifetime sensitivities in the range of $10^{34} - 10^{35}$ years with exposures up to 1000 kton$\times$year, often in quasi-background-free conditions optimal for discoveries at the few events level, corresponding to atmospheric neutrino background rejections of the order of 10^5. Multi-prong decay modes like e.g. $p \to \mu^- \pi^+ K^+$ or $p \to e^+ \pi^+ \pi^-$ and channels involving kaons like e.g. $p \to K^+ \bar{\nu}$, $p \to e^+ K^0$ and $p \to \mu^+ K^0$ are particularly suitable, since liquid Argon imaging provides typically an order of magnitude improvement in efficiencies for similar or better background conditions compared to Water Cerenkov detectors. Up to a factor 2 improvement in efficiency is expected for modes like $p \to e^+ \gamma$ and $p \to \mu^+ \gamma$ thanks to the clean photon identification and separation from π^0. Channels like $p \to e^+ \pi^0$ or $p \to \mu^+ \pi^0$, dominated by intrinsic nuclear effects, yield similar efficiencies and backgrounds as in Water Cerenkov detectors. Thanks to the self-shielding and 3D-imaging properties of the liquid Argon TPC, the result remains valid even at shallow depths where cosmogenic background sources are important. In conclusion, a LAr TPC would not necessarily require very deep underground laboratories even for high sensitivity proton decay searches.

7 Neutrino detection in liquid Argon TPC detectors

7.1 State-of-the art

Images taken with a liquid Argon TPC are comparable with pictures from bubble chambers. As it is the case in bubble chambers, events can be analyzed by reconstructing 3D-tracks and particle types for each track in the event image, with a lower energy threshold of few MeV for electrons and few tens of MeV for protons. The particle type can be determined from measuring the energy loss along the track (dE/dx) or from topology (i.e. observing the decay products). Additionally, the electronic readout allows to consider the volume as a calorimeter adding up all the collected ionization charge. The calorimetric performance can be excellent, as we will show in Section 7.2, depending on event energy and topology.

Very few real events in liquid Argon TPCs have so far been accumulated to allow a full understanding of these complex effects and their interplay. The only sample comes from a small 50 lt chamber exposed to the CERN WANF high energy neutrino beam which collected less than 100 quasi-elastic events [41].

The reconstruction of electromagnetic showers with π^0 decay was performed on the ICARUS T300 data collected on surface [42] yielding 196 candidates with a mean energy of $\sim$ 700 MeV. During the CNGS runs the ICARUS T600 at LNGS will collect about 1300 ν_μ CC (400 ν_μ NC) per 4.5×10^{19} pots (=1 nominal year). However, only about 10% of these events will be in the relevant kinematical region relevant to future neutrino oscillation experiment owing to the very high CNGS beam energy.

Almost all physics performance studies for future long-baseline experiment using liquid Argon TPC rely on a single Monte-Carlo study of π^0 rejection [43]. The sensitivity to $\sin^2 2\theta_{13}$ will directly depend on the actual π^0 rejection performance achieved with real data.

It is also clear that the energy resolution will depend on several detector parameters, including the readout pitch, the readout method chosen and on the resulting signal-over-noise ratio ultimately affecting the reconstruction of the events.

We therefore stress that significantly improved experimental studies with prototypes exposed to charged particle and neutrino beams of the relevant energies and sufficient statistics are mandatory to assess and understand these effects.

In the meantime, we give in Section 7.2 preliminary estimates for potentially achievable energy resolutions in a liquid Argon medium. The results are based on full GEANT3 [44] simulation of the

energy deposited by final state particles in the detector volume, however do not include all possible contributing effects. We show below a list of effects that need to be studied experimentally [12]:

- Neutrino interaction:
  - Fermi motion and nuclear binding energy,
  - Nuclear interactions of final state particles within the hit nucleus (FSI),
  - Vertex nuclear remnant effects (e.g. nuclear break-up signal),
  - Neutral Current (NC) π^0 event shape including vertex activity.
- Detector medium:
  - Ionization processes,
  - Scintillation processes,
  - Correlation of between amount of charge and light,
  - Charge and light quenching,
  - Hadron transport in Argon and secondary interactions,
  - Charge diffusion and attenuation due to impurity attachment.
- Readout system including electronics system:
  - signal amplification or lack thereof,
  - signal-to-noise ratio,
  - signal shaping and feature extraction.
- Reconstruction:
  - Pattern recognition
  - Background processes (NC π^0, ν_μ CC, ...) and their event shape
  - Particle identification efficiency and purity

7.2 Neutrino energy resolution in a LAr medium

As mentioned previously, the neutrino energy resolution expected in LAr medium depends on several parameters and their interplay that ultimately need to be measured experimentally.

In principle, energy and momentum conservation allow to estimate the incoming neutrino energy in the detector via a precise measurement of decay products, with the exception of the smearing introduced by Fermi motion and other nuclear effects (nuclear potential, re-scattering, absorption, etc.) for interactions on bound nucleons. In this section, we try to estimate the smearing introduced by these effects with the help of exclusive neutrino event final states distributed with the Okinoshima flux and generated with the GENIE MC [45] subsequently fully simulated with GEANT3.

Nuclear effects in neutrino interactions can be roughly divided into those of the nuclear potential and those due to reinteractions of decay products. Bound nucleons and other hadrons in nuclei are subject to a nuclear potential. The Fermi energy (or momentum) must be calculated from the bottom of this nuclear potential well, and the removal of a nucleon from any stable nucleus is always an endothermic reaction. When hadrons are produced in the nucleus, some energy is spent to take it out of this well: for a nucleon, the minimum energy is given by the nucleon separation energy (around 8 MeV), and corresponds to a nucleon at the Fermi surface. In this case, the daughter nucleus is left on its ground state. More deeply bound nucleons, leaving a hole in the Fermi sea, correspond to an excitation energy of the daughter nucleus, and an additional loss of energy of the final state products. This energy is then spent in evaporation and/or gamma deexcitation. Thus, the energy of the final state products is expected to be always slightly smaller than for interactions on free nucleons, and spread over a range of about 40 MeV. Correspondingly, the Fermi momentum is transferred to the decay products and compensated by

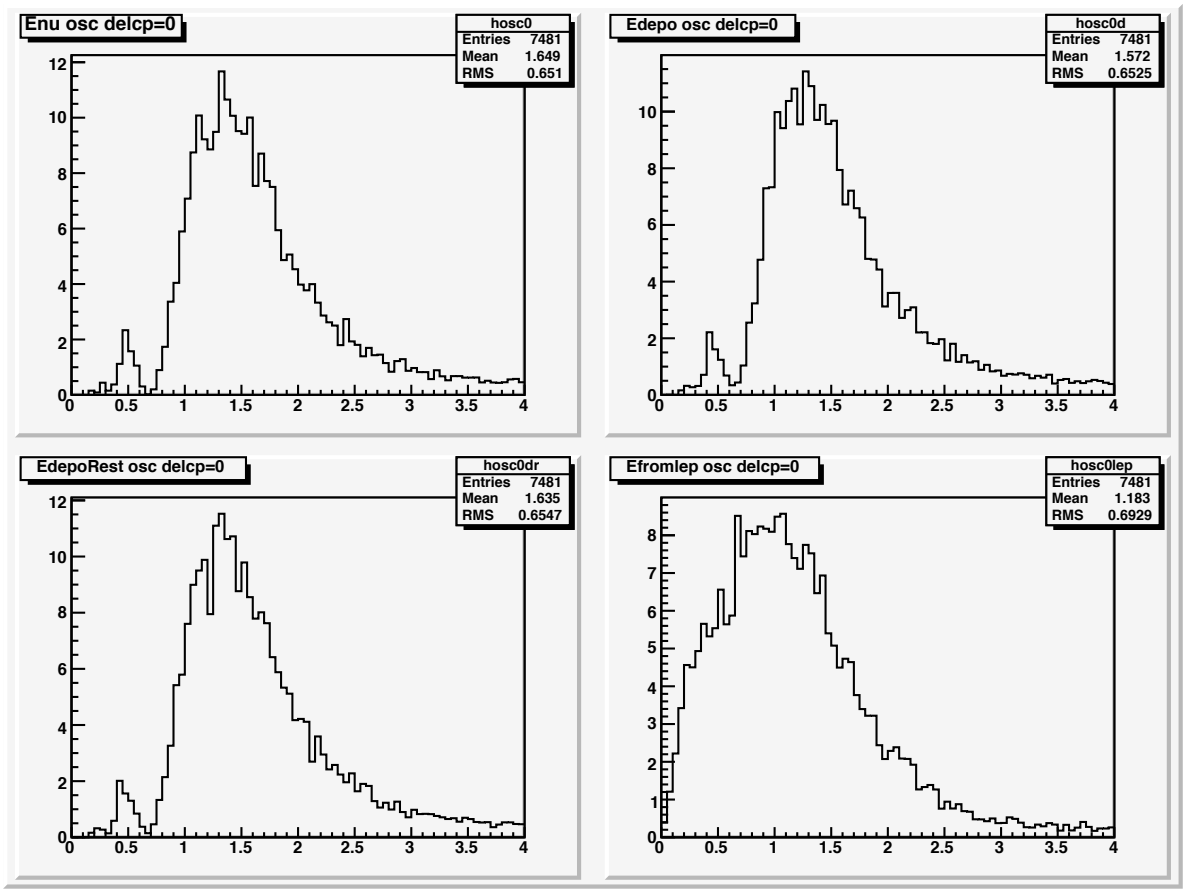

Fig. 11: Full GEANT simulations of the reconstructed neutrino energy spectra from detailed event simulation (see text) for neutrino oscillations with $\delta_{CP} = 0°$: perfect reconstruction (top-left), LAr using deposited energy(right-top), ibid but with charged pion mass correction (left-bottom) using final state lepton only (like in WC) (right-bottom) cases.

the recoil of the daughter nucleus. Additional momentum distortions come from the curvature of particle trajectories in the nuclear potential.

Reinteractions in the nuclear medium also play an important role. Interaction products can lose part of their energy in collisions, or even be absorbed in the same nucleus where they have been created. This is particularly true for pions, that have an important absorption cross section on nucleon pairs, while kaons have smaller interaction probability.

Once final state products have exited the nucleus, they will propagate in the medium with the possibility that further interactions occur.

In the case of the liquid Argon TPC, the medium is fully homogeneous and the detector is fully active. All deposited energy in the medium (above a certain threshold) will be eventually collected. Several methods can be adopted to reconstruct the neutrino energy and we list in the following three:

1. **Final state lepton:** this method, traditionally used in large Water Cerenkov detectors like Kamiokande, IMB or SK, relies on the precise measurement of the energy and direction of the outgoing lepton and kinematically constrains the incoming neutrino energy by assuming a quasi-elastic configuration:

$$E_\nu = \frac{ME_\ell - m_\ell^2/2}{M - E_\ell + p_\ell \cos\theta_\ell}$$

where E_ℓ, p_ℓ and $\cos\theta_\ell$ are the energy, momentum and scattering angle of the outgoing lepton. This method is sensitive to the final state configuration and to Fermi motion (up to $\simeq 240$ MeV/c) which randomizes the direction of the outgoing lepton.

2. **Momentum conservation:** neglecting the incoming neutrino mass, one obtains

$$E_\nu = |\vec{P}_\nu| = |\vec{p}_\ell + \sum_h \vec{p}_h - \vec{P_F}|$$

where $\vec{p}_\ell$ is the momentum of the outgoing lepton, $\vec{p}_h$ is the momentum of the outgoing hadron h and $\vec{P}_F$ is the Fermi motion of the hit nucleon (up to $\simeq 240$ MeV/c). This method is also sensitive to Fermi motion since the recoiling remnant hit nucleus (with momentum $-\vec{P}_F$) is not measured [2].

3. **Energy conservation:** using a calorimetric approach, one can sum the deposited energies of all outgoing particles. In a tracking-calorimeter this is obtained by summing the dE/dx measurements along each ionizing track to obtain the associated kinetic energies $T \equiv \int (dE/dx)dx$. One should identify final state particles in order to take into account their rest masses. This method is sensitive to the nuclear binding energy of the decay products and is intrinsically more precise than the above method relying on momenta for the energies considered here. Mathematically one can write this result as:

$$\begin{aligned} E_\nu &= E_{tot} - M = E_\ell + \sum_h E_h - M = E_\ell + \sum_h (T_h + m_h) - M \\ &= E_\ell + T_N + \sum_{\pi^\pm} (T_{\pi^\pm} + m_{\pi^\pm}) + \sum_\gamma E_\gamma + ... \end{aligned} \quad (3)$$

All methods are sensitive to potential re-interactions of the outgoing hadrons within the nucleus. In order to estimate the potential of a fully homogeneous and sensitive medium like the liquid Argon TPC, we performed full simulations of neutrino interactions: the event 4-vector are generated with the GENIE MC and final state particles (after nuclear reinteraction) were propagated through the liquid Argon medium with GEANT3. The geometry of the setup is an infinite LAr box and at this stage we have neglected charge quenching (i.e. we assume a linear response to dE/dx). We also assume a 100% efficiency to identify final state charged pions.

The achievable incoming neutrino energy resolution in the liquid Argon medium has been estimated using ν_e CC events distributed with the ν_μ flux expected at the Okinoshima location. The results, using the energy conservation method, are shown in Figure 11.

7.3 Importance of energy resolution to detect CP-violation

In order to understand the effect of resolution on physics performance, we show in this section the ν_e charged current (CC) event energy spectra and allowed regions for 100 MeV resolution case, instead of perfect resolution as shown before in Figure 5 and Figure 6. This "resolution" should include neutrino interaction effects as well as detector resolution.

If we smear the energy spectra shown in Figure 5 with Gaussian of sigma equals to 100 MeV independent from original neutrino energy, we obtain spectra shown in Figure 12. As seen easily, an energy resolution below 100 MeV is crucial since the robustness of the neutrino oscillation is directly determined by the visible second oscillation peak around 400 MeV in the energy spectrum. For resolution like in Water Cerenkov detector case, the second peak is hidden by the smearing of the 1st oscillation maximum peak.

[2] We point out that if one uses the knowledge on the direction of the incoming neutrino, the total (missing) transverse momentum can be kinematically constrained to zero, thereby providing a handle compensate for the transverse component of the Fermi motion. The longitudinal component of the momentum, which is not negligible at low neutrino energies, remains however undetermined.

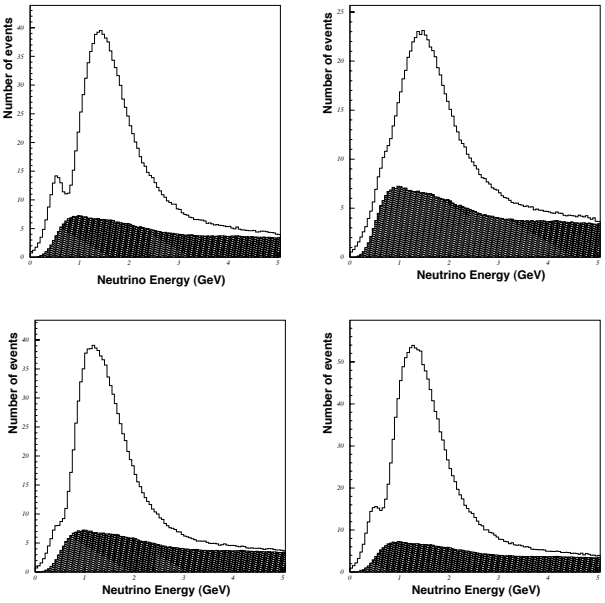

Fig. 12: Energy spectra assuming Gaussian 100 MeV smearing. δ_{CP} = 0° (top-left), 90° (right-top), 180° (left-bottom), 270° (right-bottom) cases.

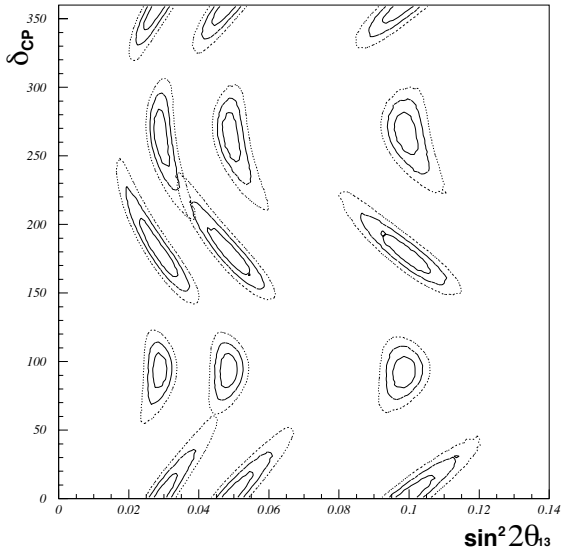

Fig. 13: Allowed regions in the 100 MeV resolution (Gaussian sigma) case. Twelve allowed regions are overlaid for twelve true values, $\sin^2 2\theta_{13}$=0.1, 0.05, 0.02, and δ_{CP}=0°, 90°, 180°, 270°, respectively.

Allowed region is then extracted for 100 MeV resolution case. The expected ν_e CC energy spectra is shown in Figure 12. The parameter fit results are shown in Figure 13.

One obvious but important issue to be pointed out is the robustness of the fitting.The fit procedure shows that results could also be extracted with the 100 MeV resolution: this result is as expected statistically; however, we stress that in this case the second oscillation maximum peak visible is hardly visible in Figure 12. Hence, we think it is mandatory to keep an energy resolution less than 100 MeV as goal for the credibility of this experiment.

8 The GLACIER detector design

The GLACIER concept is scalable to a single detector unit of mass 100 kton: it relies on a cryogenic storage tank developed by the petrochemical industry (LNG technology) and on a novel method of operation called the LAr LEM-TPC. The design is actually scalable, in the sense of Table 3: the far detector should have a total active mass of about 100 kton and could be realized with a single 1x100 kton configuration, or 3x40 kton, or even 4x 30 kton. As an example, we show the parameters envisioned for a single tank 100 kton detector in Table 4.

Liquefied Natural Gas (LNG, $\geq 95\%$ CH_4) is used when volume is an issue, in particular, for storage. The technical problems associated to the design of large cryogenic tanks, their design, construction and safe operation have already been extensively addressed and solved by the petrochemical industry over several decades. Many large LNG tanks are in service, about 300 worldwide in 2003, and there is an increased demand on LNG as alternative source of energy. The LNG tank volumes vary from 70'000 to 200'000 m^3 with erection times from 2 to 5 years. The tanks, classified according to their containment type: single, double or full containment, are defined by international design codes and standards (BS7777, EN1473, API std 620). Hundreds of large LNG tanker ships transporting volumes up to 145'000 m^3 cross the oceans every years.

The LNG industry and in particular LNG tanks have an excellent safety record. During the last 60

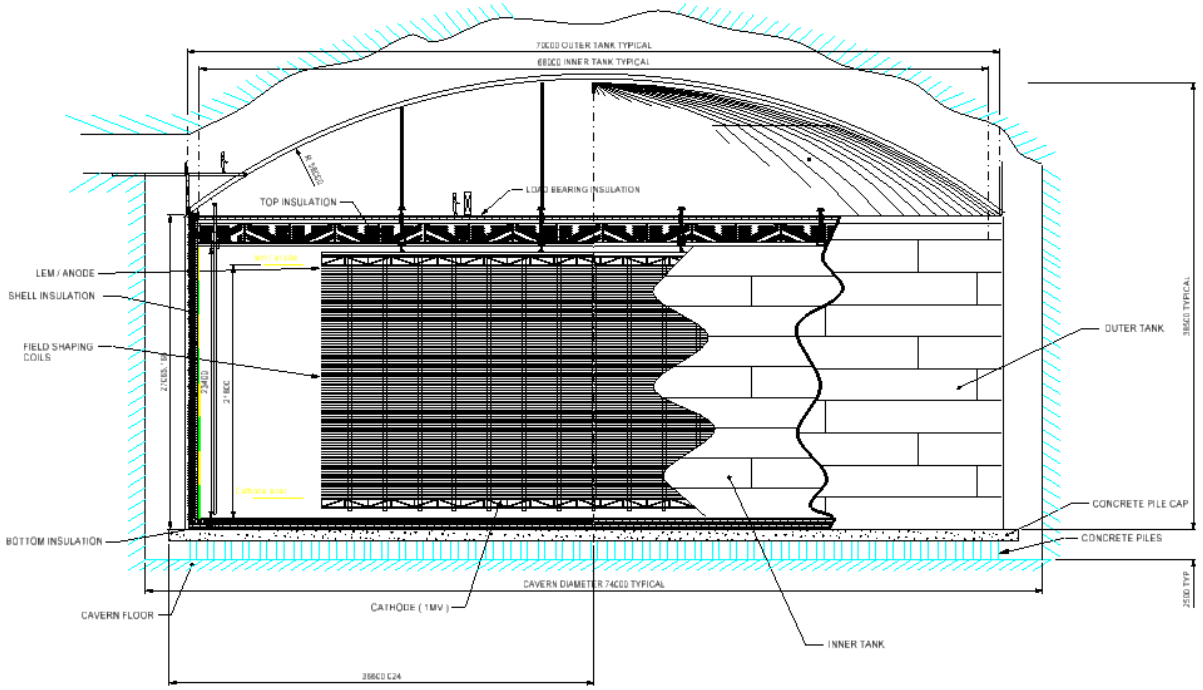

Fig. 14: Design of a 100 kton liquid Argon GLACIER tank developed in Collaboration with Technodyne International Limited [46].

years there have been only two spontaneous ruptures of large refrigerated tanks (in 1944 and 1977). In the first, the cause was attributed to brittle fracture due to the steel used and the second was due to a failure of a weld that had been repaired following a leak the previous year. Nowadays severe leaks of LNG are simply discounted as a mode of failure. Internal leaks and vapor release are more frequent and often correlated to refilling procedures with new LNG. Another source of accidents are seismic events. This excellent safety record is a result of several factors. First, the industry has technically and operationally evolved to ensure safe and secure operations. Technical and operational advances include everything from the engineering that underlies LNG facilities to operational procedures to technical competence. Second, the standards, codes and regulations that apply to the LNG industry further ensure safety.

Already in 2004 we have appointed the Technodyne International Limited, UK [46], an expert consulting company in the design of LNG tanks, to initiate a feasibility study in order to understand and clarify the issues related to the operation of a large underground LAr detector. The preliminary Technodyne study was sufficient to understand that LNG storage tank could be adequately extrapolated

	20 kton	**30 kton**	**40 kton**	**100 kton**
Tentative time scale	?			
Diameter active argon (m)	40	50	60	70
Drift length (m)	10	10	10	20
Active mass (ton)	17592	27488	39583	107753
Readout area (m2)	1257	1963	2827	3848
Maximum drift time @ 1 kV/cm	$\sim$ 5ms	$\sim$ 5ms	$\sim$ 5ms	$\sim$ 10ms
Location	Underground detector			

Table 3: Size of detectors considered at different stages. The far detector should have a total active mass of about 100 kton (e.g. 1x100 kton, 3x40 kton, 4x 30 kton, etc...)

Table 4: Summary parameters of the 100 kton GLACIER detector. From Ref. [7].

Dewar	$\Phi \approx 70$ m, height $\approx 20\ m$, passive perlite insulated, heat input ≈ 5 W/m^2
Argon Storage	Boiling argon, low pressure (< 100 mb overpressure)
Argon total volume	73118 m^3 (height = 19 m),ratio area/volume$\approx$15%
Argon total mass	102365 TONS
Hydrostatic pressure at bottom	≈ 3 atm
Inner detector dimensions	Disc $\Phi \approx 70$ m located in gas phase above liquid phase
Electron drift in liquid	20 m maximum drift, HV= 2MV for E=1 kV/cm, $v_d \approx$ 2 mm/μs, max drift time ≈ 10 ms
Charge readout views	LEM-TPC; 2 independent perpendicular views, 3 mm pitch, with charge amplification
Scintillation light readout	Yes (trigger), 1000 immersed WLS-coated 8"PMT
Visible light readout (option)	Yes (Cerenkov light), 27000 immersed 8"PMTs or 20% coverage, single photon counting capability

to the case of liquid Argon. The boiling points of LAr and CH4 are 87.3 and 111.6 K and their latent heat of vaporization per unit volume is the same for both liquids within 5%. The main differences are that (a) LNG is flammable when present in air within 5 to 15% by volume while LAr is not flammable (b) the density of LAr is 3.3 times larger than LNG, hence the tank needs to withstand higher hydrostatic pressure. This is taken into account in the engineering design. The estimated boil-off in the tank is 0.04%/day. Other cryogenic aspects have been discussed in Ref. [7].

For the requirements the recommended design – See Figure 14 – is the full containment composed of an inner and an outer tank made from steel and of the following principal components:

1. A 1m thick reinforced concrete base platform
2. Approximately one thousand 600mm diameter 1m high support pillars arranged on a 2m grid. Also included in the support pillar would be a seismic / thermal break.
3. A 1m thick reinforced concrete tank support sub-base.
4. An outer tank made from stainless steel, diameter 72.4m. The base of which would be approximately 6mm thick. The sides would range from 48mm thick at the bottom to 8mm thick at the top.
5. 1500mm of base insulation made from layers of felt and foamglas blocks.
6. A reinforced concrete ring beam to spread the load of the inner tank walls.
7. An inner tank made from stainless steel, diameter 70m. The base of which would be approximately 6mm thick and the sides would range from 48mm thick at the bottom to 8mm thick at the top.
8. A domed roof with a construction radius of 72.4m attached to the outer tank
9. A suspended deck over the inner tank to support the top-level instrumentation and insulation. This suspended deck will be slightly stronger than the standard designs to accommodate the physics instrumentation. This in turn will apply greater loads to the roof, which may have to be strengthened, however this is mitigated to some extent by the absence of wind loading that would be experienced in the above ground case.
10. Side insulation consisting of a resilient layer and perlite fill, total thickness 1.2m.
11. Top insulation consisting of layers of fibreglass to a thickness of approximately 1.2m.

Within LAGUNA, a more detailed design is being developed in Collaboration with Technodyne. In addition to the tank, the interface between tank and detector is being addressed.

GLACIER is based on concept for readout called LAr LEM-TPC [25]. LAr LEM-TPCs oper-

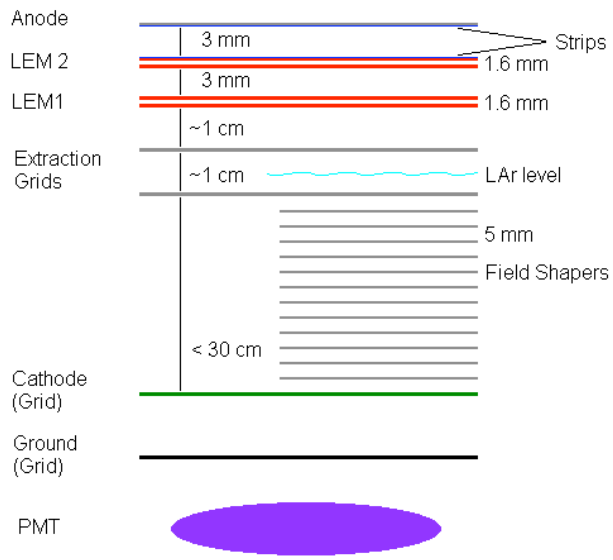

Fig. 15: Schematic of a LEM-TPC setup showing the LAr level between the two extraction grids. When operated in pure Ar gas, radioactive sources were placed on the ground grid above the PMT. From Ref. [25].

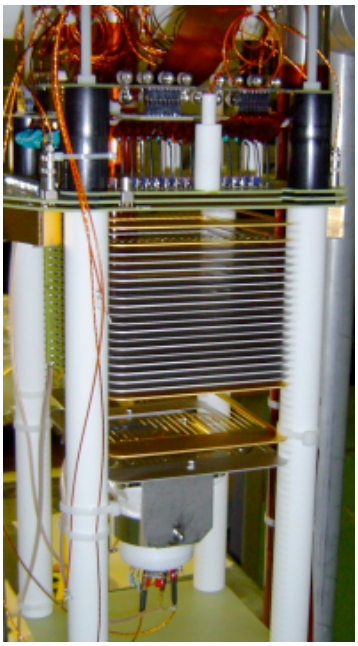

Fig. 16: Assembly of a LAr LEM-TPC prototype. From Ref. [25].

ate in double phase with charge extraction and amplification in the vapor phase. The concept has been very successfully demonstrated on small prototypes: the electron drift direction is chosen vertical for full active volume; ionization electrons, after drifting in the LAr volume, are extracted by a set of grids into the gas phase and driven into the holes of a double stage Large Electron Multiplier (LEM), where charge amplification occurs. Each LEM is a thick macroscopic hole multiplier, which can be manufactured with standard PCB techniques. The electrons signal is readout via two orthogonal coordinates, one using the induced signal on the segmented upper electrode of the LEM itself and the other by collecting the electrons on a segmented anode. The images obtained with the LAr LEM-TPC are of very high – "bubble-chamber-like" – quality, owing to the charge amplification in the LEM and have good measured dE/dx resolution. Compared to LAr TPCs with immersed wires, whose scaling is at least limited by mechanical and capacitance issues of the long thin wires and by signal attenuation along the drift direction, the LAr LEM-TPC is an elegant solution for very large liquid Argon TPCs with long drift paths and mm-sized readout pitch segmentation. Low detection thresholds are possible and the method could in principle be generalized to a 3D pixelized readout.

The general technique of electron multiplication via avalanches in small holes is attractive because (1) the required high electric field can be naturally attained inside the holes and (2) the finite size of the holes effectively ensures a confinement of the electron avalanche, thereby reducing secondary effects in a medium without quencher. The gain (G) in a given uniform electric field of a parallel plate chamber at a given pressure is described by $G \equiv e^{\alpha d}$ where d is the gap thickness and α is the Townsend coefficient, which represents the number of electrons created per unit path length by an electron in the amplification region. The behavior of this coefficient with pressure and electric field can be approximated by the Rose and Korff law: $\alpha = A\rho\, e^{-B\rho\,/E}$ where E is the electric field, ρ is the gas density, A and B are the parameters depending on the gas. Electron multiplication in holes has been investigated for a large number of applications. The most extensively studied device is the Gas Electron Multiplier (GEM) [47], made of 50–70 μm diameter holes etched in a 50 μm thick metalized Kapton foil. Stable operation has been shown with various gas mixtures and very high gains. An important step was the operation of the GEM in pure Ar at normal pressure and temperature. Rather high gas gains were obtained, of the order

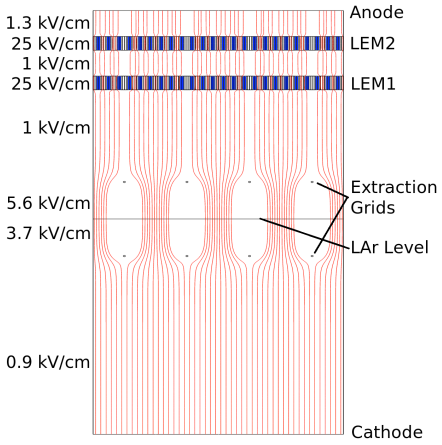

Fig. 17: Electric field lines in the double phase operation. From Ref. [25].

of 1000, supporting evidence for the avalanche confinement to the GEM micro-holes. The successes of the GEMs triggered the concept of the LEM or THGEM, a coarser but more rigid structure made with holes of the millimeter-size in a millimeter-thick printed circuit board (PCB).

In order to study the properties of the LEM and the possibility to reach high gains in double phase, we have performed extensive R&D on several prototypes [24]: We have built several LEM prototypes using standard PCB techniques from different manufacturers. Double-sided copper-clad (16 μm layer) FR4 plates with thicknesses ranging from 0.8 mm to 1.6 mm are drilled with a regular pattern of 500 μm diameter holes at a relative distance of 800 μm. By applying a potential difference on the two faces of the PCB an intense electric field inside the holes is produced.

A first single stage prototype demonstrated a stable operation in pure Ar at room temperature and pressure up to 3.5 bar with a gain of 800 per electron. Measurements were performed at high pressure because the density of Ar at 3.5 bar is roughly equivalent to the expected density of the vapour at the temperature of 87 K. Simulations of the LEM operation were performed using the MAXWELL (field calculations) and MAGBOLTZ (particle tracking) programs. The results obtained were in good agreement with the experiment. This suggested the use of the same formalism of the parallel plate chamber by replacing the gap thickness d by the effective amplification path length within the holes, called x, which can be estimated with electrostatic field calculations as the length of the field plateau along the hole. The gain is then expressed as $G_{LEM} = e^{\alpha x}$, where α is the first Townsend coefficient at the maximum electric field E inside the holes. For example, simulations indicate that $x \simeq 1$ mm for a LEM thickness of 1.6 mm, hence, $\alpha(cm^{-1}) \simeq \ln G/(0.1\ cm)$.

Double stage LEM configurations were tested in pure Ar at room temperature, cryogenic temperature and in double phase conditions. Tests in an Ar/CO_2 (90%/10%) gas mixture were also performed to compare the results with those obtained in pure Ar. The double-stage LEM system demonstrated a gain of $\sim 10^3$ at a temperature of 87 K and a pressure of $\sim$1 bar. The double-phase operation of the LEM proved the extraction of the charge from the liquid to the gas phase.

A $\sim$3 lt active volume LAr LEM-TPC, as shown schematically in Figure 15, was constructed and successfully operated. A LAr drift volume of 10x10 cm^2 cross section and with an adjustable depth of up to 30 cm is followed on top by a double stage LEM positioned in the Ar vapour at about 1.5 cm from the liquid. Ionization electrons are drifted upward by a uniform electric field generated by a system of field shapers, extracted from the liquid by means of two extraction grids positioned across the liquid-vapour interface and driven onto the LEM planes. The extraction grids were constructed as an array of parallel stainless steel wires of 100 μm diameter with 5 mm spacing. A cryogenic photomultiplier (Hamamatsu R6237-01) is positioned below the drift region and electrically decoupled from the cathode

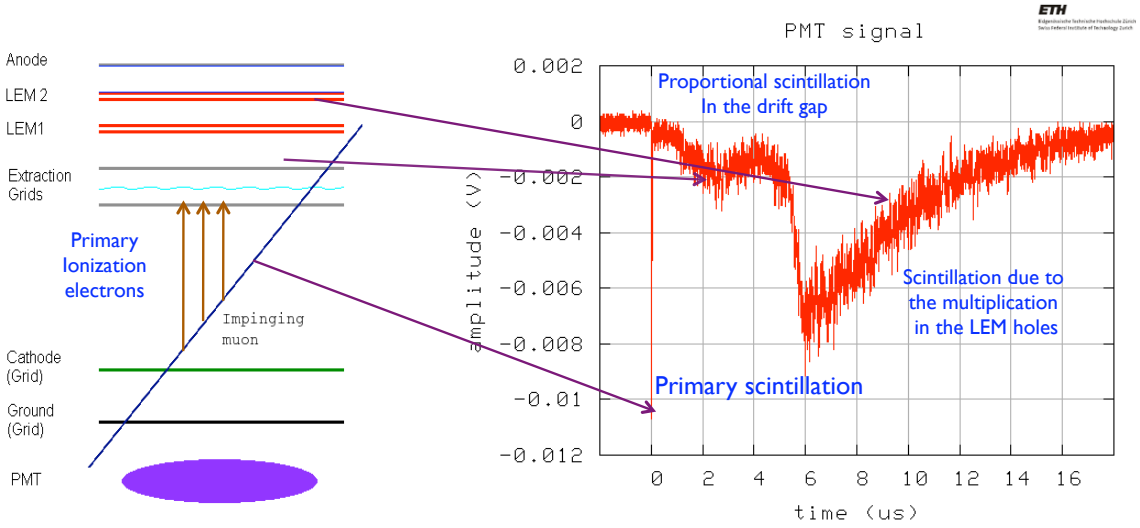

Fig. 18: Typical signal waveform of the immersed PMT Hamamatsu R6237-01.

at high voltage by a grid close to the ground potential. The photomultiplier is coated with tetraphenylbutadiene (TPB) that acts as wavelength shifter for 128 nm photons of Ar scintillation.

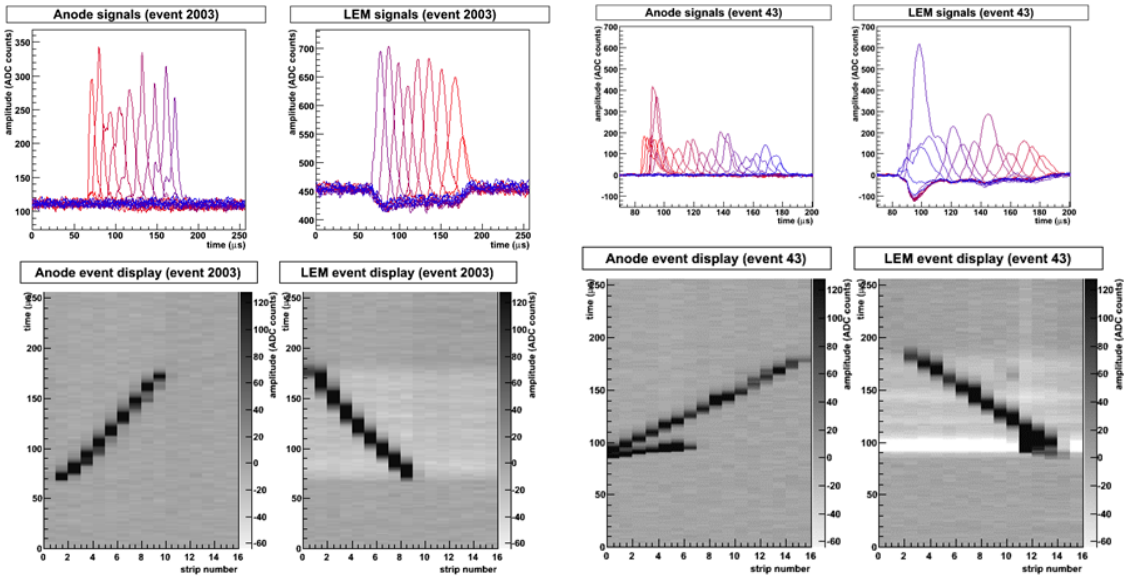

Fig. 19: Cosmic ray events as seen in the 3 lt LAr LEM-TPC at CERN.

Ionization electrons undergo multiplication into a first LEM plane and the resulting charge is then driven into a second LEM plane for further multiplication. The amplified charge is readout by measuring two orthogonal coordinates, one using the induced signal on the segmented upper electrode of the second LEM itself and the other by collecting the electrons on a segmented anode. In this first production both readout planes are segmented with 6 mm wide strips, for a total of 32 readout channels for a $\sim$10x10 cm^2 active area. Transverse segmentations down to 2–3 mm will be tested in the near future.

Signals from LEM and anode strips are decoupled via high voltage capacitors and routed to a signal collection plane placed a few centimeter above the anode. Each signal line is equipped with a surge arrester to prevent damaging the preamplifiers in case of discharges. The detector is housed inside a vacuum tight dewar and Kapton flex-print are used to connect the signal lines on the signal collection

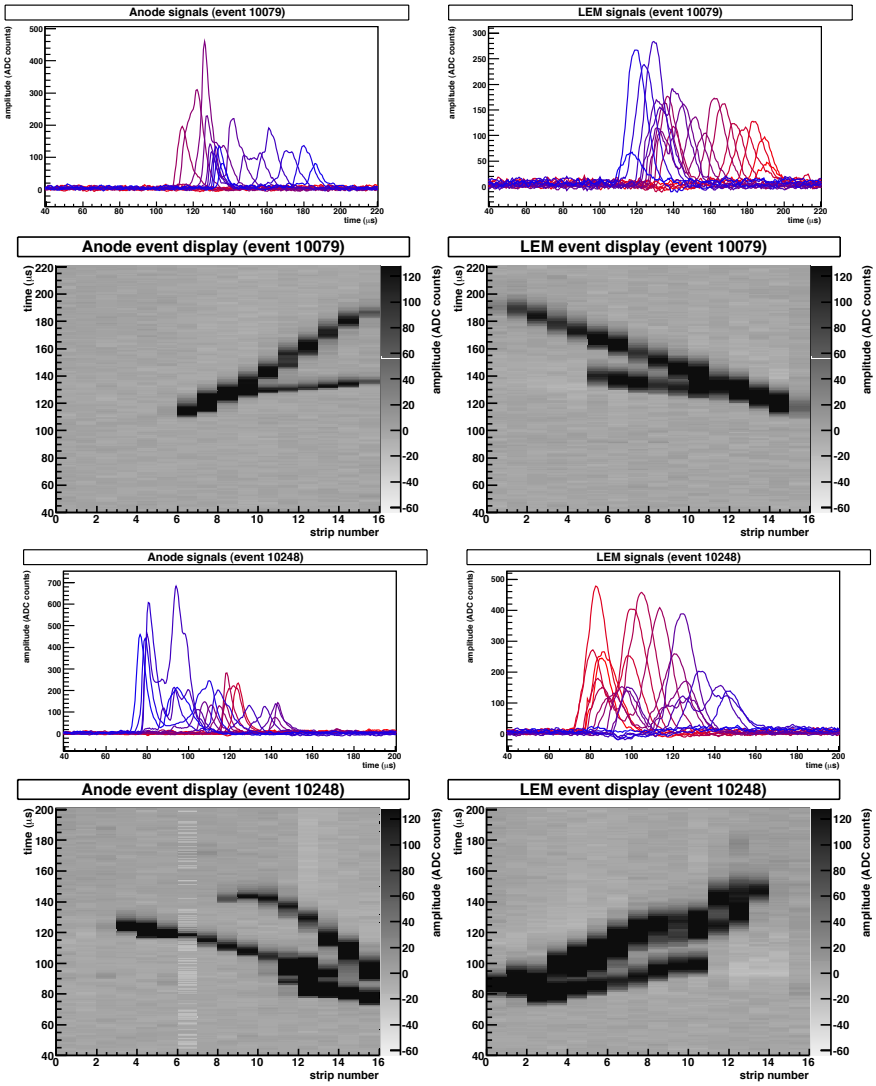

Fig. 20: Multi-tracks cosmic ray events as seen in the 3 lt LAr LEM-TPC at CERN.

board to the external readout electronics. The flex-prints exit the dewar through a slot cut in an UHV flange and sealed with a cryogenic epoxy-resin to maintain vacuum tightness.

Figure 17 shows the electric field lines from the cathode to the anode for the double phase operation. The electric fields are set increasingly from the drift region towards the anode such that fields lines starting at the cathode reach the anode (transparency).

In double phase operation the device gain was set to about 10. In this mode of operation, the PMT signal proved to be very useful in order to analyse the faith of primary ionization electrons (See Figure 18): a fast light peak indicated the direct scintillation of the crossing cosmic muon. A second light peak, shifted in time if the ionizing track did not cross the liquid surface, corresponded to the proportional scintillation (luminescence) in the high field region in the vapour just above the liquid. A third peak was interpreted as light produced during the multiplication avalanche, which escapes the LEM holes. Indeed, the size of the 3rd light peak was correlated with the electric field inside the LEM. Examples of cosmic muon tracks are shown in Figures 19 und 20 . The distribution of released charge per unit length from reconstructed cosmic muons using the anode signals is shown in Fig. 21 with a superimposed fitted Landau distribution.

Ionizing radiation in liquid noble gases leads to the formation of excimers in either singlet or

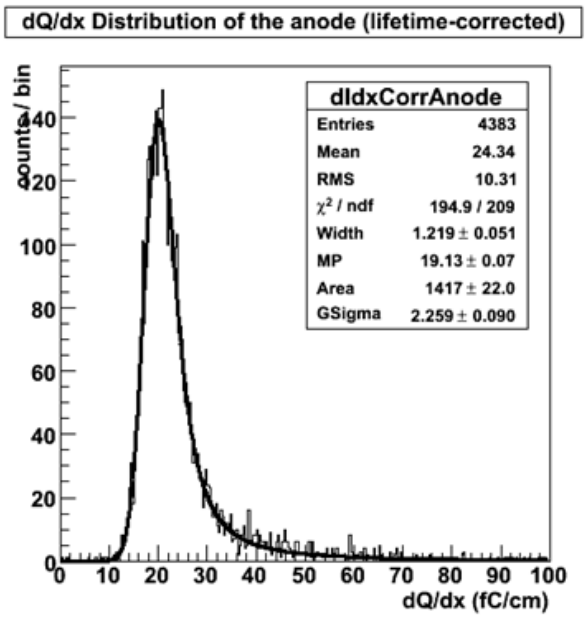

Fig. 21: Performance of 1 mm thick single stage thick GEM operating at 3.6 kV: Landau distribution from crossing muons.

triplet states [48, 49], which decay radiatively to the dissociative ground state with characteristic fast and slow lifetimes ($\tau_{fast} \approx 6$ ns, $\tau_{slow} \approx 1.6\mu$s in liquid argon with the so-called second continua emission spectrum peaked at 128 ± 10 nm [50]). Scintillation light readout provides information on events occurring in the detector. The correlation between detected light and the arrival of the charge furnishes the T_0 of the event, defining the coordinate along the drift direction. For pulsed beam events, the triggering allows to suppress backgrounds.

Large VUV sensitive PMTs (e.g. MgF_2 windowed) are not commercially available, the use of reflectors coated with a wavelength shifter (WLS) along with standard bialkali photomultiplier tubes (PMTs) is an economical realisation of an efficient readout system [27]. With about 40'000 γ's emitted per MeV deposited (at zero field) the number of PMTs does not need to be very large. We consider that about 1000 8" PMTs will be sufficient for the 100 kton GLACIER.

Liquid Argon has very similar Cerenkov light emission properties than water and also similar physical properties in terms of radiation lengths, interaction lengths, etc.. hence the events in liquid Argon look very much the same as those in water and the techniques developed for the reconstruction and analysis of Water Cerenkov detectors could in principle be "transposed" to the liquid argon case.

9 Further R&D steps towards GLACIER

Since 2008, ETHZ and KEK groups are tightly collaborating towards the realization of a very large 100 kton-scale detector. Several critical issues have been identified since several years and are subject to intense R&D efforts. As part of the R&D path to successfully design and propose the far detector on Okinoshima, several detectors of growing size are being considered. The characteristics of these detectors, either under construction or planned, are summarized in Table 5.

We summarize in the following the main areas of investigations:

1. the readout system based on the novel technique of the LAr LEM-TPC is being further studied and perfected on larger area.
2. the drift HV system based on a Cockroft-Walton voltage multiplier has been successfully tested on

	ArDM 1t	**6m3**	**250L**	**150 ton**	**1 kton**
Tentative time scale	construction	2011 ?	2010 ?	?	
Diameter active argon (m)	0.8	1.8	0.7	5	12
Drift length (m)	1.2	1.1(2.5?)	0.4	5	10
Active mass (ton)	0.85	10	0.25	137	1583
Readout area (m2)	0.5	2	0.32	20	113
Max. drift time @ 1 kV/cm	$\sim$0.6 ms	$\sim$1.25 ms	$\sim$ 0.2ms	$\sim$ 2.5ms	$\sim$ 5ms
Location	CERN	CERN	J-PARC	CERN or J-PARC	CERN or J-PARC
Cosmic rate / m^2 / drift	~ 0.1	~ 0.2	< 0.1	~ 0.4	~ 0.8
Total cosmics / drift	~ 0.25	~ 0.5	< 0.1	~ 8	~ 95

Table 5: Size of detectors considered at different stages. Surface operation precludes sensitive searches for proton decay and/or the study of non pulsed neutrino sources.

a prototype immersed in LAr and a 500 kV circuit will be further tested in the ArDM experiment;

3. new modern solutions for electronic readout have been developed in collaboration with industry (CAEN);
4. large scale liquid purification is being developed in collaboration with industry;
5. the design, construction and filling of the tank is being further studied and designed with the engineering company Technodyne within the LAGUNA design study;
6. safety aspects are being addressed in a work package of the LAGUNA design study.

In addition, it is proposed to expose a LAr TPC detector of about 6 m^3, operated in double-phase, to test beams in CERN SPS North Area [51] and to construct an engineering prototype on the 1 kton-scale [13], that could provide important physics outputs.

Beyond these efforts, we believe that a 1 kton scale device is the appropriate choice for a full engineering prototype of a 100 kton detector. The chosen size for the prototype is the result of two a priori contradictory constaints: (1) the largest possible detector as to minimize the extrapolation to 100 kton (2) the smallest detector to minimize timescale of realisation and costs. A 1 kton detector can be built assuming the GLACIER design with a 12 m diameter and 10 m vertical drift. From the point of view of the drift path, a mere factor 2 will be needed to extrapolate from the prototype to the 100 kton device. Hence, the prototype will be the real demonstrator for the long drifts. At the same time, the rest of the volume scaling from the 1 kon to the 100 kton achieved by increasing the diameter to about 70 m, can be realized noting that (a) large LNG tanks with similar diameters and aspect ratios already exist (b) the LAr LEM-TPC readout above the liquid will be scaled from an area of 80 m^2 (1 kton) to 3800 m^2 (100 kton). This will not require a fundamental extrapolation of the principle, but rather only pose technical challenges of production.

However, given its magnitude, the 1 kton scale prototype can provide more than an engineering test if it is fully instrumented. We are at present investigating the possibilities to locate this detector near J-PARC such that it could measure the J-PARC neutrino beam (and incidentally provide redundant information on the J-PARC neutrino beam compared to the existing complex at ND280 (NGRID and off-axis detector) prepared for T2K). A neutrino beam exposure at J-PARC would have the advantage that the efforts undertaken by the T2K Collaboration to predict the neutrino flux could be used in this unique setup to precisely measure neutrino exclusive cross-sections with a bubble-chamber like detector.

10 J-PARC beam exposure of the 250L chamber

The actual physics performance of the detectors will directly depend their ability to reconstruct, measure and identify low energy particles. In particular electron separation from abundant π^0 background will

be crucial. It is mandatory to consider dedicated test beam campaigns, to test and optimize the readout methods and to assess the calorimetric performance of liquid Argon detectors. The proposed test beam will address the following points:

1. **Electron, neutral pion, charged pion, muon reconstruction**: A crucial feature of the LAr TPC is a very fine sampling, which should deliver unmatched performances in particle identification and reconstruction. The reconstruction of electrons, neutral and charged pions and muons will be demonstrated. The obtained results will allow to further optimize the readout parameters for future large detectors.
2. **Electron/π^0 separation**: A crucial feature of the LAr TPC is the possibility to precisely measure and identify electrons from neutral pion backgrounds. The experimentally achievable separation will be demonstrated by inserting a hydrogenate target inside the detector in order to collect a significant sample of charge exchange events $\pi^- p \rightarrow n + \pi^0$. The obtained results will allow to further optimize the readout parameters for future large detectors.
3. **Calorimetry**: A specific feature of the LAr TPC is its 100% homogeneity and full sampling capabilities. As an extension of the measurements performed in above, more refined measurements with low energy particles (0.5-5 GeV/c $e/\mu/\pi$) will yield actual calorimetric performance and determine the ability to reconstruct full neutrino events in the GeV-range. These results will play an important role in future projects involving low energy neutrino beams or sensitive searches for proton decay and complement direct measurements in a low energy neutrino beam.
4. **Hadronic secondary interactions**: If sufficient statistics is collected, an exclusive final state study of pion secondary interactions will be attempted. Comparison of the data obtained with MC (e.g. GEANT4) will allow to cross-check and eventually tune these models. These results are relevant for running experiments (e.g. T2K).
5. **Stopping muons and pions:** If sufficient low momenta are achieved, then a sample of charge-selected stopping muons and pions will be studied in order to assess the imaging of the decay chains (for positive particles) and of the capture (for negative particles).

We are therefore planning to test the performance of the LAr LEM TPC using a 250L-scale test detector. The goal of this experiment is:

– Establish the technique to build the double phase LAr LEM TPC with 150kg active volume and 40 cm drift length.
– Measure detector performance for charged particle beam (e,mu,pi,K) of 100-1000 MeV/c
– Observe real neutrino event

10.1 Description of the 250L cryostat

Figure 22 shows a picture of the 250L cryostat. The cryostat already exists and is originally build as a prototype liquid Xenon calorimeter for MEG ($\mu \rightarrow e\gamma$) experiment [52]. The cryostat consists of two transverse cylindrical vessels (inner vessel and outer vessel). The inner vessel is meant to be filled with liquid Argon and has $\sim$70 cm diameter and $\sim$100 cm length. Thus the volume of the cryostat is about 400L. Maximum size of cuboid which can fit inside the inner vessel is $50 \times 50 \times 100$ cm^3 (250L). The volume between inner and outer vessels is for vacuum insulation and also super insulator (30 layers of aluminum myler film) is inserted to reduce thermal radiation.

Total heat input of the cryostat is estimated to be $\sim$50W at liquid Argon temperature (90K), which is extrapolated from measured heat input of 30W at liq.Xe temperature (165K).

Figure 22(right) shows a 3D drawing of the cryostat. The dimensions are shown in Figure 23. There are 4 flanges to access to the inner volume. Two top flanges are used for mounting cryogenic system and TPC signal readout feed through respectively. The front flange is used to insert TPC detector

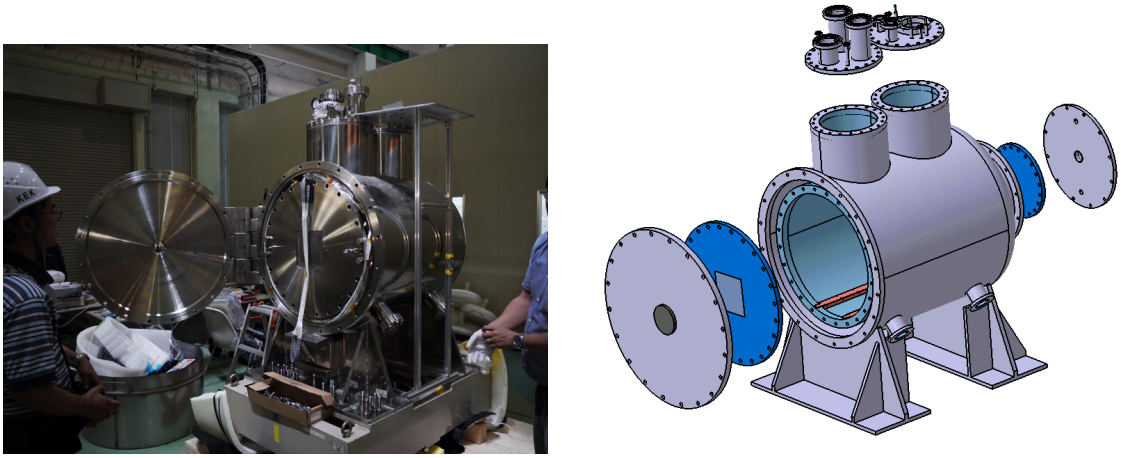

Fig. 22: (left) Photograph of the 250L cryostat; (right) exploded view of the vessel components.

into the vessel. Also there is a 5 cmx5 cm beam window at the center of the front flange. Material thickness of the beam window is 0.13 X_0. 1 back flange is connected to vacuum pump for vacuum insulation and also high voltage feed through.

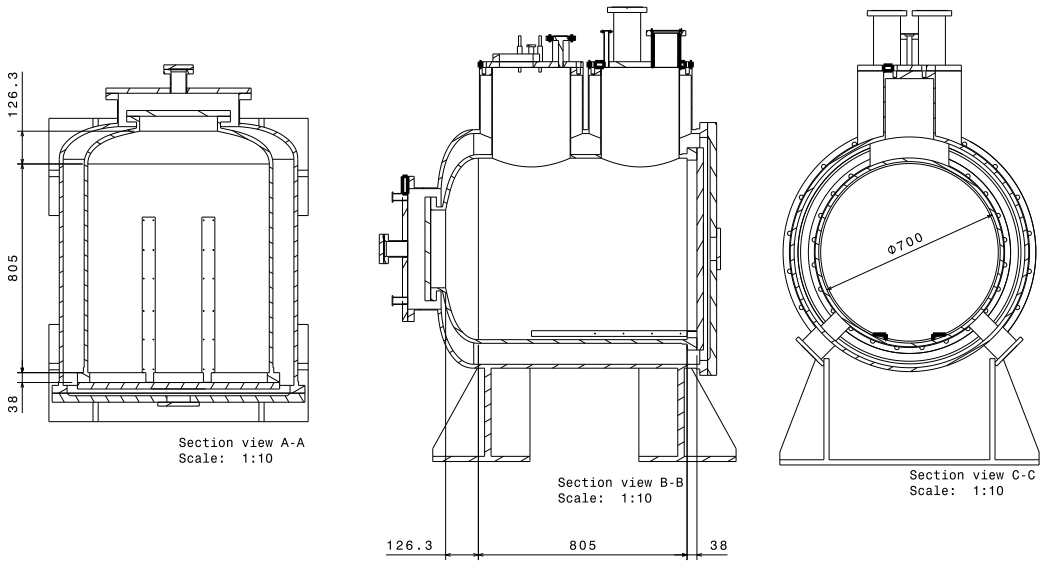

Fig. 23: 2D drawing of the 250L vessel and chamber

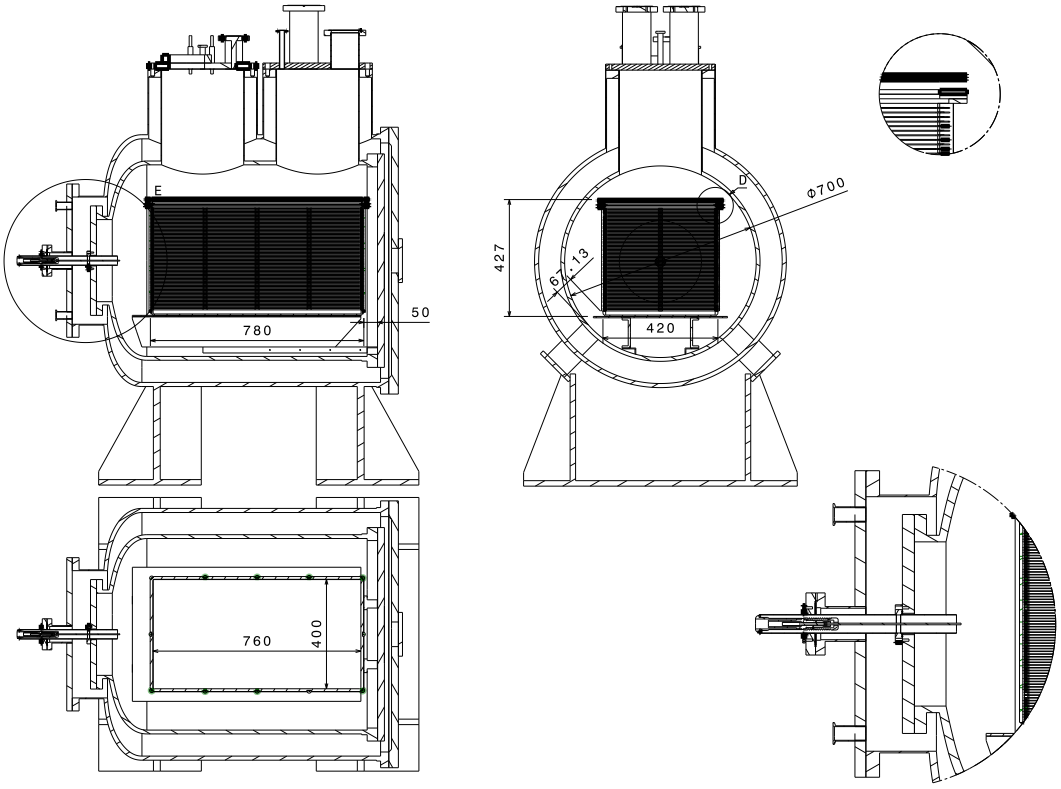

Fig. 24: 2D drawings of the vessel with the LAr LEM-TPC chamber and the high-voltage feed-through.

10.2 TPC for 250L

The TPC for the 250L will be newly built in a way to make maximal use of the available space inside the existing vessel (see Figure 24). However, we have taken care to minimize risks associated to electrical discharges against the inner walls of the vessel, in particular in the region of the cathode. The design and assembly of the chamber profits largely from the experience gained in the context of the ArDM experiment at CERN. Although of smaller volume, the 250L TPC will however represent an opportunity to develop further the adopted technical solutions. The main parameters of the chamber are summarized in Table 6. The active readout volume is $40 \times 40 \times 76$ cm^3 which corresponds to a total mass of about 170 kg. The chamber will be oriented such that the beam crosses along the longest dimension of the chamber. In term of radiation length, the active argon provides about 5 X_0 and about 1 interaction length.

The cathode will be placed at the bottom of the volume and the field shapers will provide an uniform electric drift field which will bring the ionization electrons towards the top of the chamber at the interface between the liquid and the vapor. There, a set of grids will extracts the electrons into the vapor phase. We anticipate the use of one LEM layer of about 1 mm thickness and look for effective gains in the range of 10. The anode will be made a x-y-strips embedded in a kapton foil with a readout pitch of 3 mm. The strips will be oriented in a way that both x and y views make an angle of 45^o w.r.t. the incoming beam direction.

The above design and its assembly will extensively rely on the expertise gained in ArDM. The CERN EN/ICE Workshop will be involved and will benefit from the participation of the ETHZ group in the CERN RD51 collaboration [28].

A custom-built HV feed-through will be used (it has already been manufactured at ETHZ and

CERN). It will be inserted into the vessel from the back curve dome. It will bring the tension for the cathode, which we plan to set up to 40 kV in order to create a drift field of 1 kV/cm.

The TPC will have about 576 readout channels in total. We will use kapton cables similar to those specially designed at ETHZ and produced at the CERN PCB workshop for the ArDM experiment. In this context, we have successfully demonstrated the high compactness of this design and its performance in cold and in ultra-high-vacuum. The signals will be connected to charge preamplifiers similar to those developed for ArDM and digitized with the specially developed CAEN SY2791 system.

Tentative parameters for 250L detector	
Fiducial mass	170 kg
Total LAr mass	$\sim$ 400 kg
Field cage dimensions	$42 \times 42 \times 78$ cm^3
Fiducial volume	$40 \times 40 \times 76$ cm^3
Drift field	1 kV/cm
Max. drift voltage	40 kV
Readout method	Double phase, LEM-TPC
Readout segmentation	2 independent LEM-TPCs, 40×38 cm^2 each
Readout pitch	3 mm in x & y
Number of readout channels	288 per LEM-TPC 576 in total
LEM-TPC effective gain	~ 10

Table 6: Parameters of the 250L LAr LEM-TPC chamber.

10.3 Cryogenic and Purification System for the 250L Setup

In the 250L setup, maximum drift distance of the ionization electron is about 40 cm. Thus we need to achieve at least 0.5 ppb of liquid Argon purity so that the attenuation of the signal does not causes significant problem. Figure 25 shows a schematic drawing of the cryogenic and purification system for the 250L test. The procedure to obtain and keep high purity liquid argon in the vessel is as follows,

- Evacuate the inner vessel using molecular turbo pump ($<10^{-4}$ Pa).
- Pre-cool the vessel using a GM cryocooler and a LN2 heat exchange coil. Cold power of the GM cryocooler is 160 W at liquid Argon temperature (90K) and the LN2 heat exchange coils provide up to 300 W.
- Fill the vessel with liquid Argon after passing the purification cartridge (Oxysorb). At this point, we expect to achieve $\sim$ 5 ppb of liquid Argon purity.
- Further purification by recirculating gas Argon. Evaporate liquid argon inside the cryostat using cryogenic heater, and purify the gas Argon, then liquefy using the GM cryocooler and the LN2 coil. The system is designed so that 1 full volume of the liquid Argon inside the vessel can be recirculated in a day.

By using this system, we will be able to obtain liquid Argon with 0.5 ppb purity, which is sufficient to obtain high quality given the drift length of the setup.

10.4 Proposed exposure at K1.1BR and beam requirements

As discussed in Section 2, the LAr TPC will have excellent sensitivity for observing nucleon decay particularly into charged kaon mode ($p \to K^+\nu$, etc.). In the two body decay of $p \to K^+\nu$ the kaon possess a monochromatic momentum of 340 MeV/c (neglecting Fermi motion). The exposure at K1.1BR will

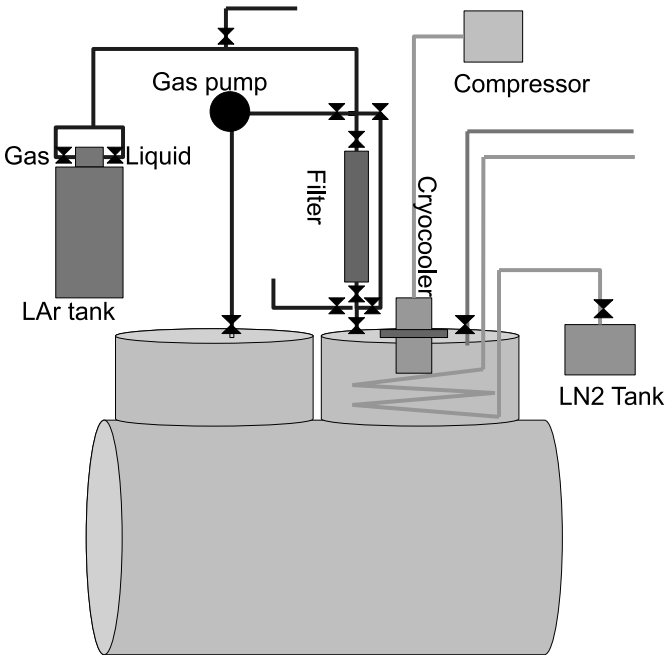

Fig. 25: Cryogenic and purification system diagram of the 250L test.

provide an important sample in order to collect a good sample of kaons and study features and reconstruction algorithms for these particles, including for the stopping ones, their decay products. Therefore, we hereby propose an exposure of the 250L LAr TPC detector to the charged Kaon with momentum range of 300–800 MeV/c at J-PARC K1.1BR beamline.

Figure 26 shows schematic view of the K1.1BR beamline and Figure 27 shows expected particle yield right after the target. In this section we describe the test procedure and an requirement to the beamline so that we can achieve good measurement.

Figure 28 shows a typical event display of simulated event when injecting a charged kaon with momentum of 340 MeV/c to the 250L detector. The configuration for simulating the event is as follows;

- Charged Kaon with 340 MeV/c momentum ($\equiv$+x direction)
- Detector size $40 \times 40 \times 80$ cm^3
- Readout strip: perpendicular to beam direction ($\equiv$y direction)
- Readout pitch 3 mm
- For simplicity, we use only 1 dimensional strip readout, and assume y position of the hit is know with good precision.
- Drift electron direction: $\equiv$+z, drift speed 1.4 cm/μs (E=1 KV/cm)
- Drift electron signal is also segmented to z direction with 3 mm (2.1 μs) pitch.

In this event, the charged kaon stops after $\sim$15 cm, then decay into $\mu^+\nu$. The muon escapes from the detector before loosing all the energy. Figure 29 shows a typical event of $K^+ \rightarrow e^+\nu\pi^0(\rightarrow \gamma\gamma)$ decay mode. One can identify an electron(positron) from the K^+ stopping point and two separated vertex for γ interaction (1 conversion and 1 Compton scattering).

As we can see from these events, the 250L detector is large enough for containing all the Kaon stopping vertex. For its decay products, the detector may not contain all the energies, but still gives great insight for understanding the detector performance. For example, Figure 30 shows dE/dx (energy deposition / path length) distribution of each strip for all hits including the initial Kaon and decay daughters

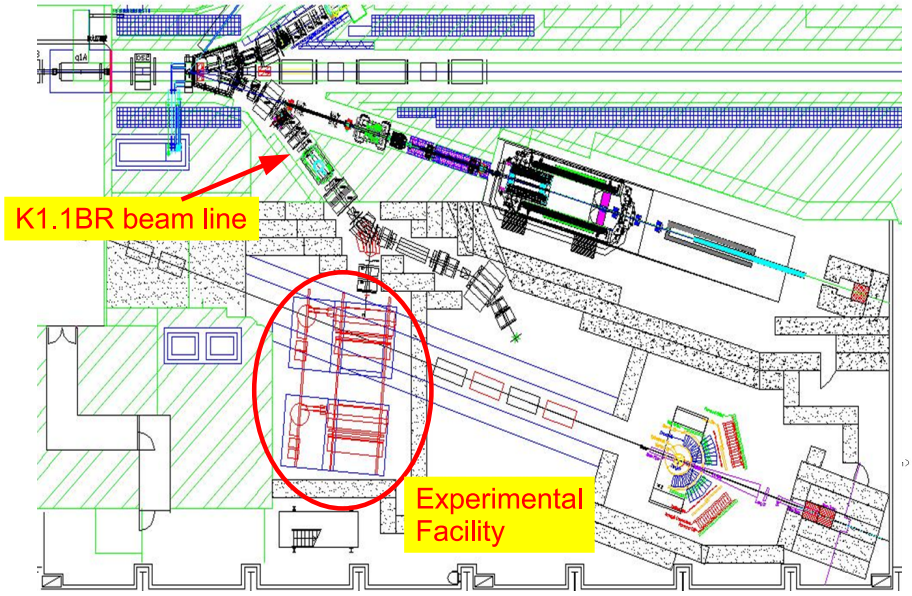

Fig. 26: Schematic view of the K1.1BR beamline at J-PARC hadron beamline

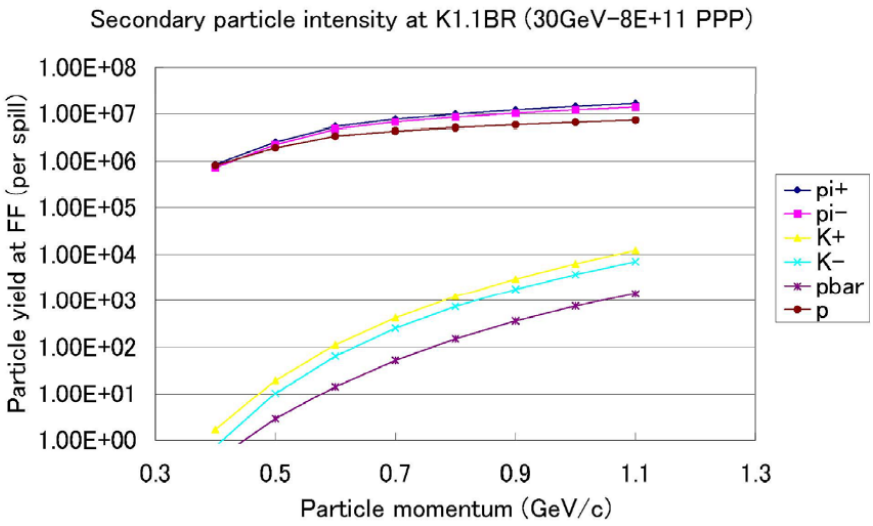

Fig. 27: Particle yield at K1.1BR beamline.

(top plot). The plot has double peak structure, and the first peak is corresponding to MIP ($\sim$ 2 MeV/cm). Bottom plot is the same plot, but separately for different particle species (Red/Blue/Cyan/Purple histograms are corresponding to $K/\mu/\pi$/e, respectively). Muon, pion and electron are around MIP, and kaon consist the second peak as expected. Measuring this distribution will give a good test of the particle identification performance of the LAr TPC.

Figure 31 shows path length (top) and energy deposition (bottom) of the K^+ inside the detector for 300–800 MeV/c input K^+ momentum. Range of the K^+ inside the liquid Argon is $\sim$15 cm (43 cm)

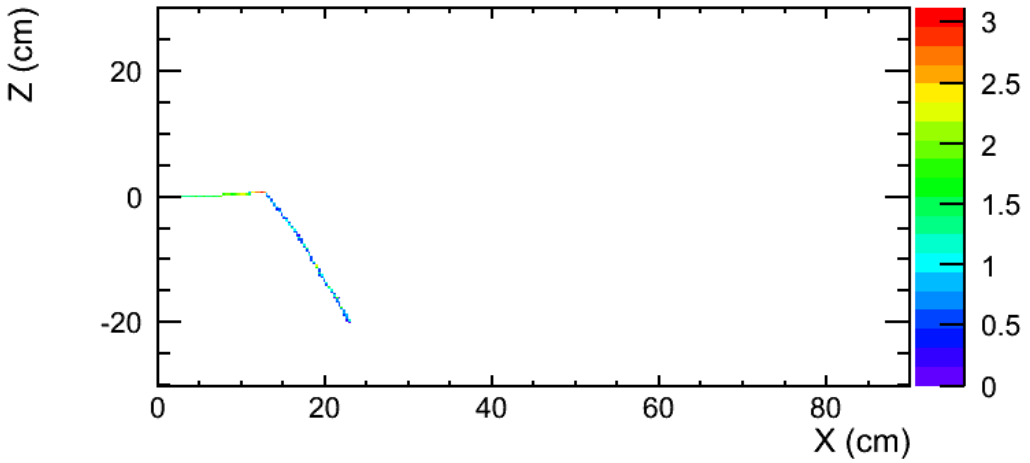

Fig. 28: A display of the simulated event of 340 MeV/c K^+ injected to the 250L detector. In this event, the kaon decays into $K^+ \to \mu\nu$.

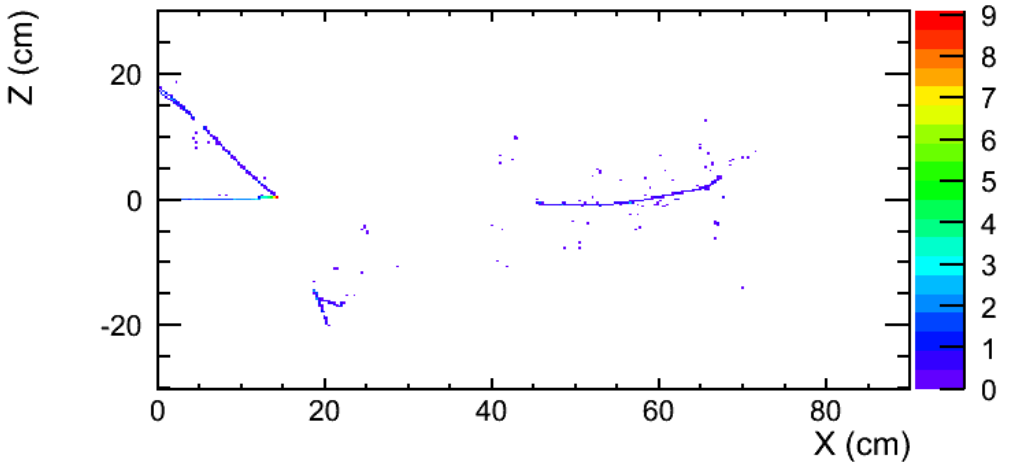

Fig. 29: A display of the simulated event of 340 MeV/c K^+ injected to the 250L detector. In this event, the kaon decays into $K^+ \to e^+\nu\pi^0(\to \gamma\gamma)$.

for 340 MeV/c (500 MeV/c). If momentum of K^+ is greater than 700 MeV/c, kaon penetrates the 80 cm of liquid Argon and escape from the detector. This is why the path length is saturated at 80 cm, and the energy deposition rather decreases for higher momentum kaons.

The followings are requests to the K1.1BR beamline:

- Figure 30 corresponds to 1000 simulated kaons. We think 1000 events would be enough to understand the detector performance for one specific configuration. We would like to accumulate data with different test configurations. For example, beam momentum, detector HV, readout pitch, etc.
- the LAr TPC has slow drift speed ($\sim$ mm/μs), it takes $\sim$ 400 μs the ionization electron drifts from bottom to top of the 40 cm drift region. if the beam rate is too high, the detector can not distinguish daughter particles from different beam particles. Thus latency of the beam needs to be more than $\sim$ ms (beam rate less than kHz).

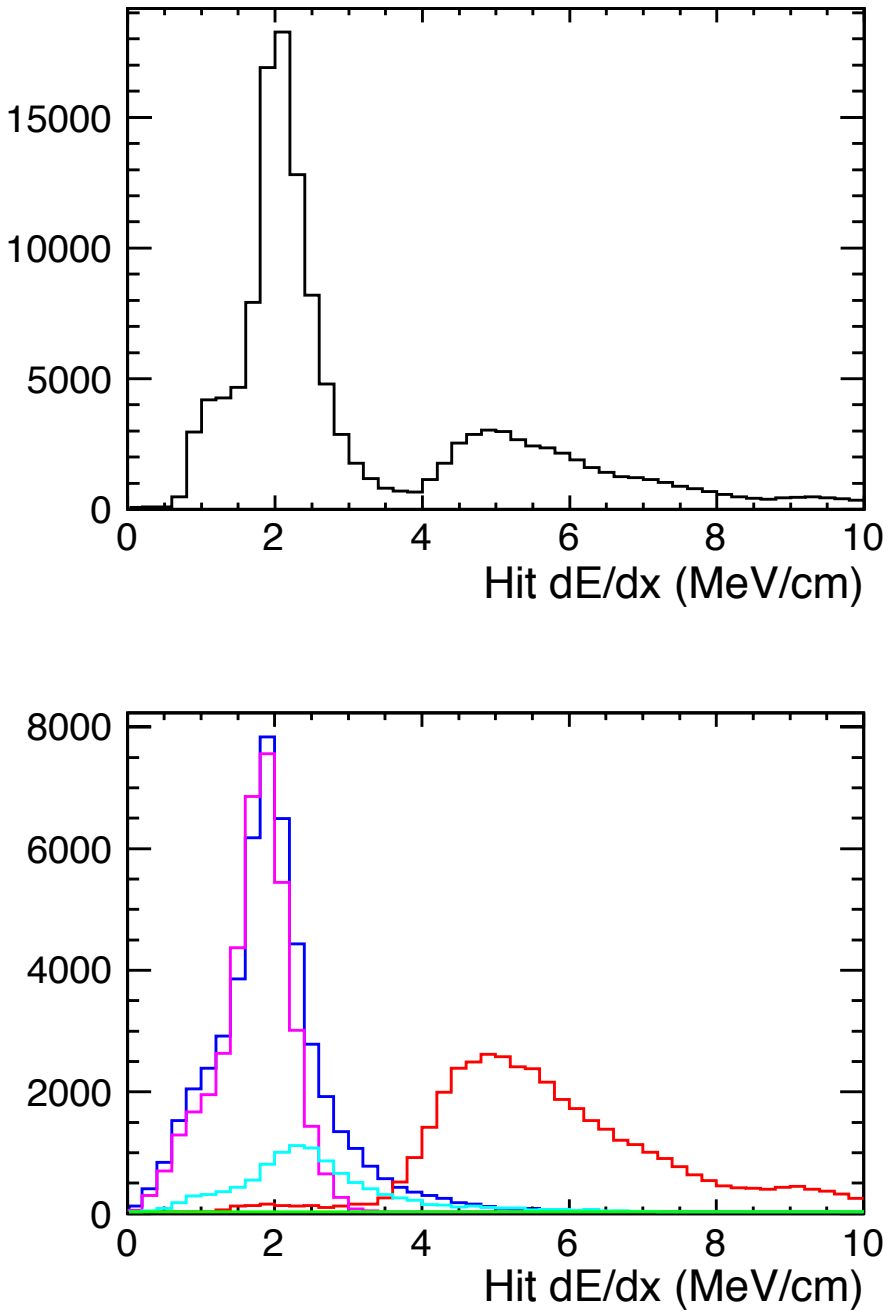

Fig. 30: dE/dx distribution of the TPC signal (3 mm readout pitch) for all the particles (top) when injecting 340 MeV/c K^+. Red/Blue/Cyan/Purple histograms are corresponding to $K/\mu/\pi$/e, respectively.

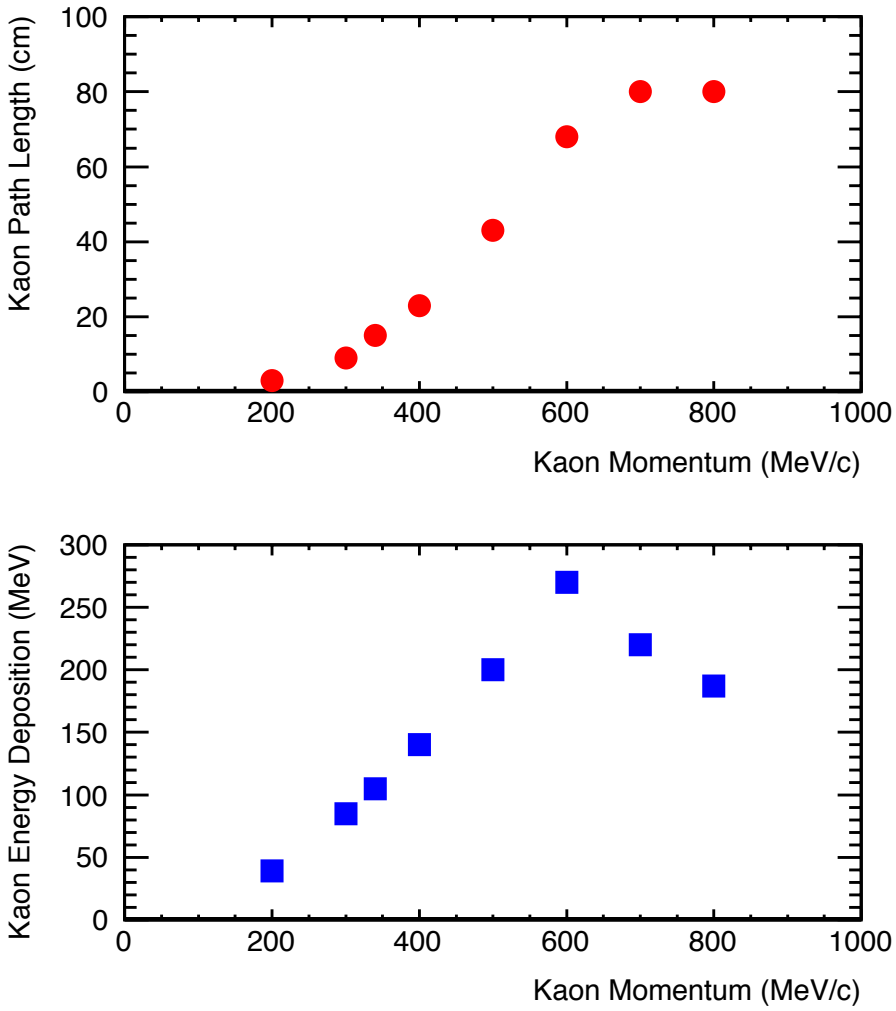

Fig. 31: Path length (top) and energy deposition (bottom) of the K^+ inside the detector for 300–800 MeV/c input K^+ momentum.

– the LAr TPC should be able to identify beam particle type by itself, but it is helpful if beam can provide good kaon purity, and beamline equipment can provide PID information.
– the LAr TPC can NOT determine drift start time (t_0) without a photodetector to measure the prompt scintillation light, so it is helpful if the beamline equipment can provide beam position and timing information particle by particle.

11 Conclusions

In this document, we present a strong physics case for a new long baseline experiment composed of a 100 kton liquid Argon TPC detector located in the region of Okinoshima. Such a detector would detect the existing J-PARC neutrino beam at a distance of 658 km and an off-axis angle of 0.76^o. We argued that this setup provides excellent conditions to study the θ_{13} and δ_{CP} phase phenomenology. With a realistic increase of the MR power from the baseline 750 kW to a 1.66 MW, the experiment would determine in 5 years the value of θ_{13} with $\delta(\sin^2 2\theta_{13}) \sim \pm 0.01$ and test CP-violation at better than 90% C.L. if θ_{13} had been previously detected in T2K, or otherwise improve the limit on θ_{13} by an order

of magnitude ($\sin^2(2\theta_{13}) \lesssim 10^{-3}$ at 90%C.L.). For a value of δ_{CP} in the region of 90^o or 270^o, the statistical significance would exceed 3σ for $\sin^2(2\theta_{13}) \gtrsim 0.02$. If θ_{13} were found, one could consider adding 5 years of antineutrino run to confirm CP-violation at $> 3\sigma$ if $\sin^2(2\theta_{13}) > 10^{-2}$.

With an underground setting, the experiment will also extend the sensitivity to nucleon lifetime in the range of $10^{34} - 10^{35}$ years, depending on the decay mode, in a region where several theoretical models predict its existence. It will also detect natural sources of neutrinos (atmospheric, supernovae, from DM annihilation, etc.).

At the present state of demonstrated scaling of the technique, the construction and operation of a 100 kton liquid Argon TPC certainly represents a technological challenge. However, several critical issues have been identified since several years and are subject to intense R&D efforts. Much of the emphasis has been on the development of a new readout scheme which can be scaled to large sizes, and on the assessment of large vessels based on the LNG tanks technology providing storage for large quantities of ultra pure liquid Argon. In this context, the successful operation of the LAr LEM TPC shows excellent prospects for becoming the standard readout method for very large detectors, providing large signal-to-noise ratio (and hence excellent physics performance) also for chambers of large sizes and with very long drift paths.

Since 2008, ETHZ and KEK groups are tightly collaborating towards the realization of a very large detector. We have developed a coherent and synergetic R&D strategy, which envisions the construction and operation of prototypes at CERN and at KEK/JPARC. After successful operation of small prototypes at the 3L and 10L scales, the ETHZ and KEK groups are focusing their strengths on the construction of the 250L detector at KEK. In addition, the ETHZ group is presently commissioning the 1-ton ArDM detector at CERN.

In this context we stress the importance of dedicated experimental measurement campaigns in charged particles test beams as well as neutrino beams. Such efforts are not only needed to develop the technology but are also fundamental to gain a clear understanding of the detector response and performance.

For these reasons, we are considering a test-beam exposure of the 250L chamber into the K1.1BR beam. This proposal represents the most economic and efficient way to rapidly establish the techniques to build and operate a double phase LAr LEM TPC with 170kg active volume and 40 cm drift length at J-PARC, and in addition to assess at first instances the detector performance for charged particle beam (e,mu,pi,K) of 100-1000 MeV/c.

We consider the 250L test at JPARC K1.1BR as a very important step, fully complementary to our ongoing or planned measurements at CERN. If successful, it will motivate us to continue our investigations towards a J-PARC neutrino beam exposure, in order to collect a real set of neutrino interactions with the new LAr LEM TPC readout method.

For the medium term, we believe that construction and operation of a 1 kton scale detector will be an important milestone towards the underground 100 kton facility. If the 1 kton would be located in a neutrino beam, it would provide unique physics opportunities to study exclusive neutrino cross-sections with a truly bubble-chamber-like event imaging.

References

[1] Y. Suzuki, "Super-Kamiokande results on neutrino oscillations," Phys. Scripta **T121** (2005) 23.

[2] T. Kajita, "Recent results from atmospheric and solar neutrino experiments," Nucl. Phys. Proc. Suppl. **155**, 155 (2006).

[3] K. Eguchi *et al.* [KamLAND Collaboration], "First results from KamLAND: Evidence for reactor anti-neutrino disappearance," Phys. Rev. Lett. **90**, 021802 (2003) [arXiv:hep-ex/0212021].

[4] Q. R. Ahmad *et al.* [SNO Collaboration], "Direct evidence for neutrino flavor transformation from

neutral-current interactions in the Sudbury Neutrino Observatory," Phys. Rev. Lett. **89**, 011301 (2002) [arXiv:nucl-ex/0204008].

[5] Y. Itow *et al.*, "The JHF-Kamioka neutrino project," arXiv:hep-ex/0106019.

[6] H. Nishino *et al.* [Super-Kamiokande Collaboration], "Search for Proton Decay via $p \to e^+\pi^0$ and $p \to \mu^+\pi^0$ in a Large Water Cherenkov Detector," Phys. Rev. Lett. **102** (2009) 141801 [arXiv:0903.0676 [hep-ex]].

[7] A. Rubbia, "Experiments for CP-violation: A giant liquid argon scintillation, Cerenkov and charge imaging experiment?," arXiv:hep-ph/0402110.

[8] I. Gil Botella and A. Rubbia, "Decoupling supernova and neutrino oscillation physics with LAr TPC detectors", JCAP **0408** (2004) 001 [arXiv:hep-ph/0404151].

[9] A. G. Cocco, A. Ereditato, G. Fiorillo, G. Mangano and V. Pettorino, "Supernova relic neutrinos in liquid argon detectors", JCAP **0412** (2004) 002 [arXiv:hep-ph/0408031].

[10] A. Meregaglia and A. Rubbia, "Neutrino oscillation physics at an upgraded CNGS with large next generation liquid argon TPC detectors," JHEP **0611**, 032 (2006) [arXiv:hep-ph/0609106].

[11] A. Bueno, Z. Dai, Y. Ge, M. Laffranchi, A.J. Melgarejo, A. Meregaglia, S. Navas, A. Rubbia "Nucleon decay searches with large liquid argon TPC detectors at shallow depths: Atmospheric neutrinos and cosmogenic backgrounds," JHEP **0704**, 041 (2007) [arXiv:hep-ph/0701101].

[12] A. Badertscher, T. Hasegawa, T. Kobayashi, A. Marchionni, A. Meregaglia, T. Maruyama, K. Nishikawa and A. Rubbia "A Possible Future Long Baseline Neutrino and Nucleon Decay Experiment with a 100 kton Liquid Argon TPC at Okinoshima using the J-PARC Neutrino Facility," arXiv:0804.2111 [hep-ph].

[13] A. Rubbia, "Underground Neutrino Detectors for Particle and Astroparticle Science: the Giant Liquid Argon Charge Imaging ExpeRiment (GLACIER)," J. Phys. Conf. Ser. **171**, 012020 (2009) [arXiv:0908.1286 [hep-ph]].

[14] C. Rubbia, "The Liquid-Argon Time Projection Chamber:A New Concept For Neutrino Detector", CERN-EP/77-08(1977).

[15] S. Amerio *et al.* [ICARUS Collaboration], "Design, construction and tests of the ICARUS T600 detector," Nucl. Instrum. Meth. A **527** (2004) 329.

[16] L. Bartoszek *et al.*, "FLARE: Fermilab liquid argon experiments", arXiv:hep-ex/0408121.

[17] D. B. Cline, F. Raffaelli and F. Sergiampietri, "LANNDD: A line of liquid argon TPC detectors scalable in mass from 200-tons to 100-ktons", JINST **1** (2006) T09001 [arXiv:astro-ph/0604548].

[18] D. B. Cline, F. Sergiampietri, J. G. Learned and K. McDonald, "LANNDD: A massive liquid argon detector for proton decay, supernova and solar neutrino studies, and a neutrino factory detector", Nucl. Instrum. Meth. A **503** (2003) 136 [arXiv:astro-ph/0105442].

[19] B. Baibussinov *et al.*, "A new, very massive modular Liquid Argon Imaging Chamber to detect low energy off-axis neutrinos from the CNGS beam. (Project MODULAr)", Astropart. Phys. **29** (2008) 174 [arXiv:0704.1422 [hep-ph]].

[20] D. Angeli *et al.*, "Towards a new Liquid Argon Imaging Chamber for the MODULAr project", JINST **4** (2009) P02003.

[21] A. Marchionni, "Liquid Argon R&D", To appear in CERN Yellow Report - Future Neutrino Physics Workshop, October 2009.

[22] T. Maruyama, "LAr detector R&D in Japan", talk at NNN09, Estes Park, Oct. 2009.

[23] A. Rubbia, "ArDM: A ton-scale liquid argon experiment for direct detection of dark matter in the universe", J. Phys. Conf. Ser. **39** (2006) 129 [arXiv:hep-ph/0510320].

[24] P. Otyugova, "Development of a Large Electron Multiplier (LEM) based charge readout system for the ArDM experiment", Diss. ETH No. 17704, 2008.

[25] A. Badertscher *et al.*, "Construction and operation of a Double Phase LAr Large Electron Multiplier

Time Projection Chamber", arXiv:0811.3384 [physics.ins-det].

[26] A. Badertscher *et al.*, "Operation of a double-phase pure argon Large Electron Multiplier Time Projection Chamber: comparison of single and double phase operation," NIM A, *in press* [arXiv:0907.2944 [physics.ins-det]].

[27] V. Boccone *et al.* [The ArDM Collaboration], "Development of wavelength shifter coated reflectors for the ArDM argon dark matter detector," arXiv:0904.0246 [physics.ins-det].

[28] RD51 Collaboration, `http://rd51-public.web.cern.ch/`

[29] G. Steigman Ann.Rev.Astron.Astrophys, 14(1976)339; A.D. Sakharov Pisma Zh.ETF 5(1967)32.

[30] The LAGUNA design study is financed by the European Community FP7 Research Infrastructure "Design Studies", Grant Agreement No. 212343 FP7-INFRA-2007-1. See `http://laguna.ethz.ch`

[31] A. Rubbia, Document submitted to the SPC neutrino sub-panel, November 2009.

[32] M. Apollonio *et al.* [CHOOZ Collaboration], Phys. Lett. B **466**, 415 (1999) [arXiv:hep-ex/9907037].

[33] M. Freund, "Analytic approximations for three neutrino oscillation parameters and probabilities in matter," Phys. Rev. D **64**, 053003 (2001) [arXiv:hep-ph/0103300].

[34] A. Cervera, A. Donini, M. B. Gavela, J. J. Gomez Cadenas, P. Hernandez, O. Mena and S. Rigolin, "Golden measurements at a neutrino factory," Nucl. Phys. B **579**, 17 (2000) [Erratum-ibid. B **593**, 731 (2001)] [arXiv:hep-ph/0002108].

[35] K. Hagiwara, N. Okamura and K. i. Senda, "Physics potential of T2KK: An extension of the T2K neutrino oscillation experiment with a far detector in Korea," Phys. Rev. D **76**, 093002 (2007) [arXiv:hep-ph/0607255].

[36] `http://nuint.ps.uci.edu/nuance/`

[37] L. Wolfenstein, "Neutrino oscillations in matter," Phys. Rev. D **17** (1978) 2369.

[38] P. Huber, M. Lindner and W. Winter, "Simulation of long-baseline neutrino oscillation experiments with GLoBES," Comput. Phys. Commun. **167**, 195 (2005) [arXiv:hep-ph/0407333].

[39] J. C. Pati and A. Salam, "Unified Lepton-Hadron Symmetry And A Gauge Theory Of The Basic Interactions," Phys. Rev. D **8**, 1240 (1973).

[40] H. Georgi and S. L. Glashow, "Unity Of All Elementary Particle Forces," Phys. Rev. Lett. **32**, 438 (1974).

[41] F. Arneodo *et al.* [ICARUS-Milano Collaboration], "Performance of a liquid argon time projection chamber exposed to the WANF neutrino beam," Phys. Rev. D **74**, 112001 (2006) [arXiv:physics/0609205].

[42] A. Ankowski *et al.* [ICARUS Collaboration], "Energy reconstruction of electromagnetic showers from π^0 decays with the ICARUS T600 Liquid Argon TPC," arXiv:0812.2373 [hep-ex].

[43] Y. Ge, P.R. Sala, A. Rubbia, "e/π^0 separation in ICARUS LAr-TPC", ICARUS-TM/03-05, 2003; Yuanyuan Ge, "Study of Atmospheric Neutrino Detection in Liquid Argon Time Projection Chamber", Diss. ETH No. 16984 (2006).

[44] R. Brun *et al.*, GEANT3 Reference Manual,. CERN Program Library Long Writeup. W5013, DD/EE/84-1, 1987. For hadronic secondary interactions, we select GFLUKA.

[45] C.Andreopoulos, Nucl.Phys.B Proc.Suppl. 159:217-222, 2006; C.Andreopoulos, Act.Phys.Pol.B Vol.37,8:2349, 2006

[46] Technodyne International Limited, Unit 16 Shakespeare Business Center Hathaway Close, Eastleigh, Hampshire, SO50 4SR, see `http://www.technodyne.co.uk`.

[47] F. Sauli, "GEM: A new concept for electron amplification in gas detectors", Nucl. Instr. and Meth. A 396 (1997) 531.

[48] T. Doke, K. Masuda and E. Shibamura, "Estimation of absolute photon yields in liquid argon

and xenon for relativistic (1 MeV) electrons", http://dx.doi.org/10.1016/0168-9002(90)90011-T *Nucl. Instrum. Meth. A* **291** (1990) 617.

[49] S. Kubota, M. Hishida and J. Raun, "Evidence for a triplet state of the self-trapped exciton states in liquid argon, krypton and xenon", http://dx.doi.org/10.1088/0022-3719/11/12/024 *J. Phys. C: Solid State Phys.* **11** (1978) 2645.

[50] T. D. Strickler and E. T. Arakawa, *Optical Emission from Argon Excited by Alpha Particles: Quenching Studies* J. Chem. Phys. **41**, (1964) 1783.

[51] D. Autiero *et al.*, "Test beam exposure of a Liquid Argon TPC Detector at the CERN SPS North Area", Abstract #82, Workshop on New Opportunities in the Physics Landscape at CERN, May 2009.

[52] S. Mihara [MEG Collaboration], "R&D work on a liquid-xenon photon detector for MEG experiment at PSI," Nucl. Instrum. Meth. A **518**, 45 (2004).

Author list

A.Badertscher, A.Curioni, S.DiLuise, U.Degunda, L.Epprecht, L.Esposito, A.Gendotti, S.Horikawa, L.Knecht, C.Lazzaro, D.Lussi, A.Marchionni, A.Meregaglia, G.Natterer, F.Resnati, A.Rubbia, C.Strabel, T.Viant

ETH Zurich, 101 Raemistrasse, CH-8092 Zurich, Switzerland

T.Hasegawa, T.Kobayashi, T.Maruyama, K.Nishikawa, M.Tanaka

KEK High Energy Accelerator Research Organization, 1-1, Oho, Tsukuba, Ibaraki, 305-0801, Japan